

California Department of Fish and Wildlife
Stream Evaluation Report 2022-01

**INSTREAM FLOW EVALUATION: JUVENILE REARING OF
STEELHEAD AND COHO SALMON IN UPPER MARK WEST
CREEK, SONOMA COUNTY**

APPENDICES

TABLE OF CONTENTS

APPENDIX A: HEC-RAS 2D MODEL CALIBRATION..... 1

APPENDIX B: FIELD OBSERVATIONS 57

APPENDIX C: STREAMFLOW–HABITAT TABLES 72

ABBREVIATIONS AND ACRONYMS

2D	two-dimensional (hydraulic model)
AWS	area-weighted suitability
cfs	cubic foot (feet) per second
cms	cubic meter(s) per second
cm	centimeter(s)
CN	Courant number
DTM	digital terrain model
DWA	Diffusion Wave Approximation (2D numerical solution equation)
EG	energy gradient
FM	Full Momentum (2D numerical solution equation)
FN	Froude number
ft	foot (feet)
ft/s	foot (feet) per second
HEC-RAS	Hydrologic Engineering Center – River Analysis System
NAVD 88	North American Vertical Datum of 1988
Q	flow (discharge)
RM	roughness multiplier
SZF	stage of zero flow
VBM	vertical benchmark
WSEL	water surface elevation
XS-1	cross section 1 (at the downstream boundary of the site)
XS-2	cross section 2 (near the top of the site)

APPENDIX A: HEC-RAS 2D MODEL CALIBRATION

This Appendix presents the two-dimensional (2D) model calibration methods and results used to evaluate juvenile rearing of anadromous fish species in upper Mark West Creek. The 2D module of the Hydrologic Engineering Center's River Analysis System (HEC-RAS), Version 5.0.6 (HEC-RAS 2018), was used to perform the analysis. Three 2D models were constructed, calibrated, and validated, one for each of the study sites. The methods used to collect the field data for the 2D models are presented in the main technical report. The 2D models were used to estimate depths and velocities over a range of simulated flows. The depth and velocity raster files were exported to an Esri ArcGIS Pro environment and used to compute an index of habitat suitability that indicates suitable flow levels for rearing of juvenile steelhead and Coho Salmon.

The following sections describe the development of model inputs necessary to construct the 2D models and execute flow simulations, model calibration techniques, and validation procedures. Execution of the 2D model to simulate depth and velocity to estimate juvenile rearing involved calibrating flow-water surface elevation (WSEL) data collected in the field, estimating channel roughness using substate coding, converting topographic survey data into digital terrain models (DTMs), constructing 2D models in HEC-RAS, calibrating flow simulations over a range of flow to estimate juvenile rearing, and validating the model outputs using randomly collected depths and velocities collected in the field.

A.1 Units of Measure

The 2D modeling results are expressed in imperial units (e.g., ft). The discharge measurements and WSEL data were collected using imperial units. The topographic surveys used to develop the DTMs were performed using a metric Universal Transverse Mercator (UTM) Zone 10 projected coordinate system. Consequently, the HEC-RAS flow simulations were run using metric units for the model geometry and hydraulic parameters. The HEC-RAS hydraulic results were then converted back to imperial units for reporting.

A.2 2D Model Methodology Overview

The 2D module of HEC-RAS is a hydrodynamic model that solves for conservation of mass and momentum in the x- and y-horizontal plane using depth-averaged equations (WEST Consultants Inc 2017). The variables used to compute 2D models are WSEL, velocity in the x-direction, and velocity in the y-direction. WSEL is solved for using a

step-back approach. The downstream boundary condition is defined as a hydraulic control point with a constant WSEL corresponding to the inflow defined at the upstream boundary condition. Water depth is estimated from WSEL outputs in each cell of the computational grid. HEC-RAS solves for velocity in the x-direction and velocity in the y-direction in the horizontal plane but does not solve for velocity in the vertical z-direction.

A.2.1 Flow-WSEL Data Collection Timing

The channel geometry, substrate composition and ratings must stay stable during the 2D model data collection for any given site, including data collection for rating curve development. Flow-WSEL ratings change over time as channel-forming flows alter the substrate composition and geometry of the stream channel in both the lateral and longitudinal direction. Channel-forming flows can change the elevation and/or location of the downstream hydraulic control point or the cross-sectional profile of the transect where WSELs were measured. The stream channel must be rerated in between channel forming flow events to reestablish the rating curve.

Pressure transducers were stationed near XS-1 (cross section 1, at the bottom of the site) in each site for the 2018-2019 and 2019-2020 water years. The same flow-WSEL ratings developed for the 2D models were used to convert the pressure transducer WSEL data into a flow time series. The flow time series developed for Site 1 was used to estimate that a peak flow of over 2,000 cubic feet per second (cfs) occurred on February 27, 2019 (Figure A-1). The topographic surveying and flow-WSEL ratings needed to calibrate Sites 1 and 2 were completed prior to the peak event in February. The topographic surveys needed for Site 3 were not performed until the summer of 2019. Therefore, the flow-WSEL ratings needed for Site 3 were developed from discharge and WSEL data collected after the channel-forming flow event on February 27, 2019.

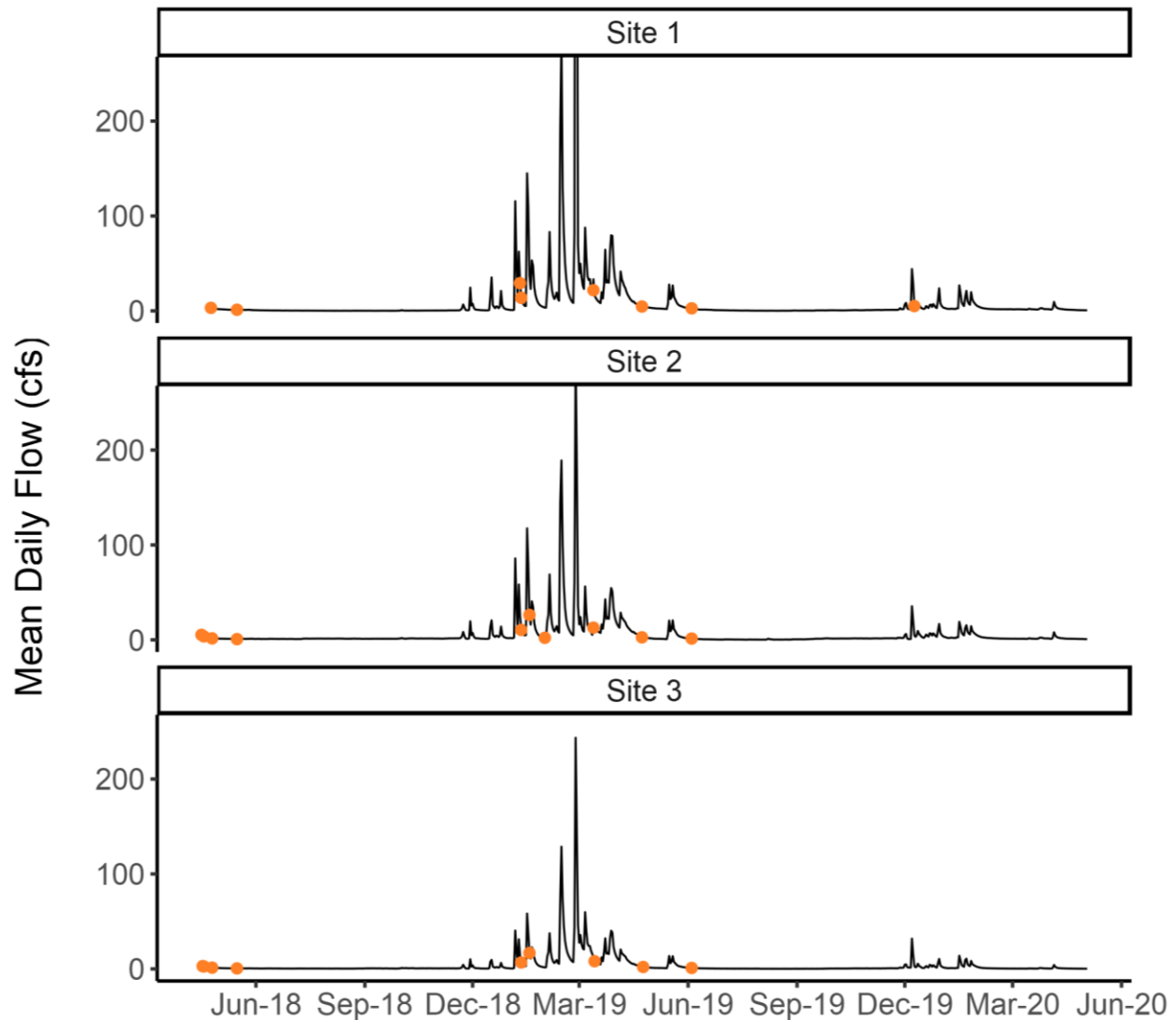


Figure A-1. Flow time series developed for each study site. Orange markers indicate when flow-WSEL data were collected. The peak flow at Site 1 on February 27, 2019, was estimated to be above 2,000 cfs.

A.2.2 Flow-WSEL Rating Curve Development at Boundary Transects

2D model calibration requires that flow and WSEL rating relationships be developed for upstream and downstream boundary conditions. Each rating relationship (rating) is created by measuring flow and WSEL over the range of flows needed to meet the study objectives. A minimum of three flow-WSEL pairs are needed to establish a rating.

The boundary transects for each site were placed in pools where the WSEL level was flat and could be reliably measured. In pools, the slope of the longitudinal water surface

is controlled by a downstream thalweg elevation point, termed the stage of zero flow (SZF; Figure A-2).

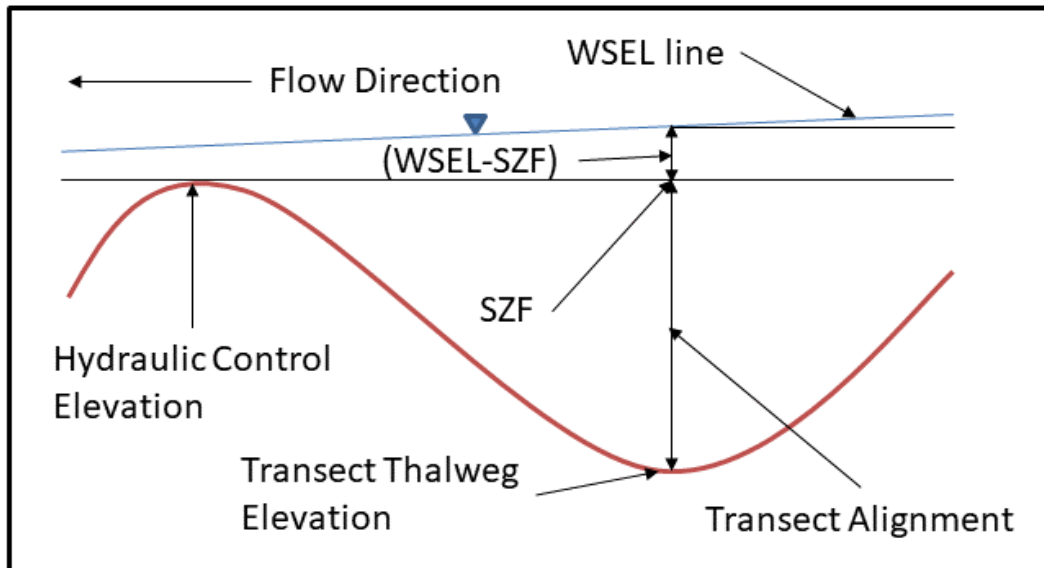


Figure A-2. SZF diagram.

The 2D model topographic surveying to create the DTMs for Sites 1 and 2 was completed in fall 2018, and surveying for Site 3 was completed in summer 2019. To construct ratings for Sites 1 and 2, flow-WSEL data were collected starting in spring 2018 and extended through January 2019 prior the channel-forming flow event in February 2019, described above. The flow-WSEL data for the Site 3 2D model was collected after the channel-forming flow event in March, April, and June of 2019.

Log-log regression was used to develop the flow-WSEL predictive rating curves. Log-log regression is an empirical method Milhous et al. (1989) used to develop hydraulic rating curves that incorporates the SZF to optimize the rating relationship as follows:

$$Q = A \times (WSEL - SZF)^{exp} \quad \text{(Equation A-1)}$$

Where:

Q = flow (cfs)

A = regression coefficient

exp = exponential regression coefficient

The above equation is converted to log-log format and a best-fit linear relationship is fitted to the data points.

A.2.3 Stream Channel Roughness and Substrate Classifications

HEC-RAS uses Manning's equation to solve for open channel flow. Manning's equation is solved for a section of channel, normal to the flow direction (Gupta 1995). The equation is provided below as follows:

$$Q = 1.486/n AR^{2/3}S^{1/2} \quad (\text{English Units}) \quad (\text{Equation A-2})$$

where

n = Manning's roughness coefficient (dimensionless)

A = cross-sectional area of the wetted channel section (ft²)

R = hydraulic radius (ft); A/P

P = wetted perimeter (ft)

S = slope of the energy grade line, estimated as the slope of the water surface.

Stream channel roughness varies with discharge (Chow 1959); typically roughness increases as flow levels recede because the ratio of cross-sectional flow conveyance area to channel roughness decreases. Manning's n is commonly specified in ranges based on the characteristics of the open channel being evaluated; for natural channels of irregular sections with pools a range of 0.04 to 0.10 is recommended for section-based, one-dimensional hydraulic models. For 2D hydraulic models, a narrower range of Manning's n values would be expected, since 2D models explicitly model the irregularity of sections in the underlying terrain. A one-dimensional model uses the Manning's n term to implicitly model more than just "roughness" – it also captures energy lost due to lateral flow and complex flow paths. A 2D model represents this energy loss explicitly (Friend and McBroom 2018).

When using a field-map approach to estimating channel roughness, ideally flow simulation would occur without any modification to the field-map values because the change in roughness due to flow level is accounted for by the variable roughness of the map. The main report describes the channel morphology of the three study sites: Site 1 is a classic meandering alluvial channel with a mixture of grain sizes ranging from deposits of fines in slow side channel pools to narrow boulder-dominated high-gradient riffles and step-runs; Site 2 maintains some elements of a meandering channel, but the channel gradient is steeper, dominated by cobble, boulder, and bedrock outcroppings; and Site 3 is a steep, narrow, boulder/bedrock-dominated channel. The stream channel roughness layers imported into HEC-RAS were multiplied by a constant roughness multiplier (RM) where necessary to calibrate flow-WSEL relationship monitored at XS-2 (cross section 2, near the top of the site).

Substrate codes were assigned to each topographic survey point. Substrate codes were assigned by visually estimating the average of particle size at the location of each survey point. The codes used to classify substrate are provided in Table A-1.

Table A-1. Substrate codes, descriptors, and particle sizes (USFWS 2011).

Code	Type	Particle Size (inches)
0.1	Sand/Silt	<0.1
1	Small Gravel	0.1–1
1.2	Medium Gravel	1–2
1.3	Medium/Large Gravel	1–3
2.3	Large Gravel	2–3
2.4	Gravel/Cobble	2–4
3.4	Small Cobble	3–4
3.5	Small Cobble	3–5
4.6	Medium Cobble	4–6
6.8	Large Cobble	6–8
8	Large Cobble	8–10
9	Boulder/Bedrock	>12
10	Large Cobble	10–12

Stream bed roughness is defined in HEC-RAS using the Manning’s n roughness coefficient n . There are two ways to assign stream channel roughness in HEC-RAS: a single n value can be assigned to the model in the 2D Flow Area menu or n can be spatially varied within the model. There are two ways to specify spatially varied roughness in HEC-RAS using the RAS Mapper utility: 1) the user can import a map of roughness values based on site conditions as polygons in a shapefile, or 2) the user can import a pre-existing gridded land cover layer. Variable roughness polygon shapefiles were developed for each site based on the substrate coding. The substrate codes were converted to n values using an equation that estimates n using median particle size as follows:

$$n = 0.048 d_{50}^{0.179} \quad (\text{ft}) \quad \text{Bray (1979)} \quad (\text{Equation A-3})$$

The version of the equation from Bray (1979) is reported here in Imperial units (ft) as presented in Jobson and Froehlich (1988) and Coon (1998). The original version of the equation was developed in metric units (Bray 1979). The substrate coding assigned to each topographic survey point was used as a proxy for median particle size in that portion of the channel and converted to n values using this equation (Table A-2). For

example, a substrate code of 2.4 was assumed to have a median particle size of 3 inches.

Table A-2. Substrate codes converted to n values.

Substrate Code	n
0.1	0.020
1	0.031
1.2	0.033
1.3	0.035
2.3	0.036
2.4	0.037
3.4	0.038
3.5	0.039
4.6	0.041
6.8	0.044
8	0.045
9	0.048
10	0.046
Mean	0.038
Median	0.039

Each topographic survey point and associated n value were imported into ArcGIS as a shapefile. The points were converted into Thiessen polygons (Figure A-3), which is defined as a polygon where any location within each polygon is closer to its associated point than to any other point (ESRI 2020). Once in the RAS-Mapper utility, the shapefile was converted into a raster using the same cell size as the DTM, 0.1 m (Figure A-4).

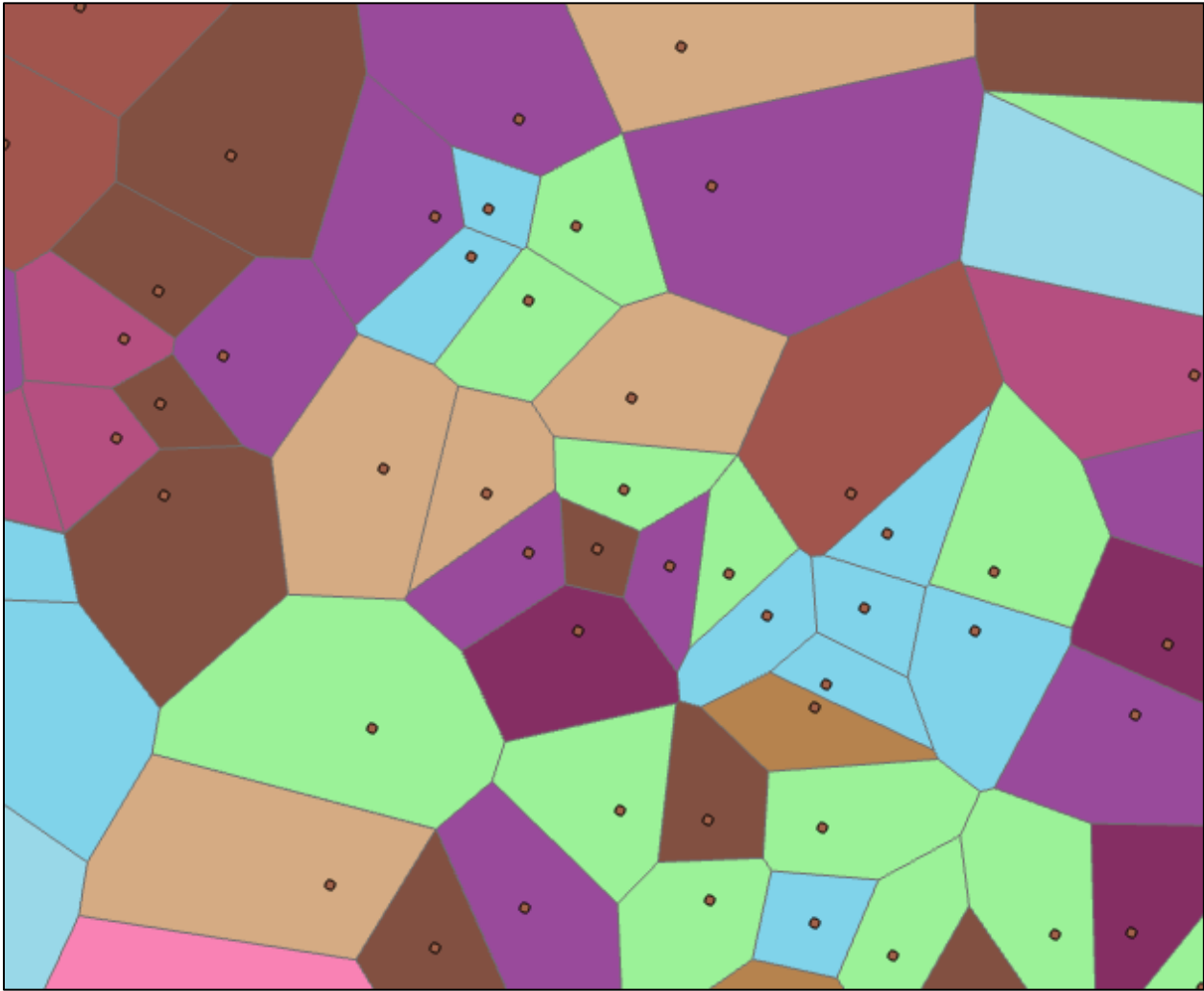


Figure A-3. Point values converted to Thiessen polygons.

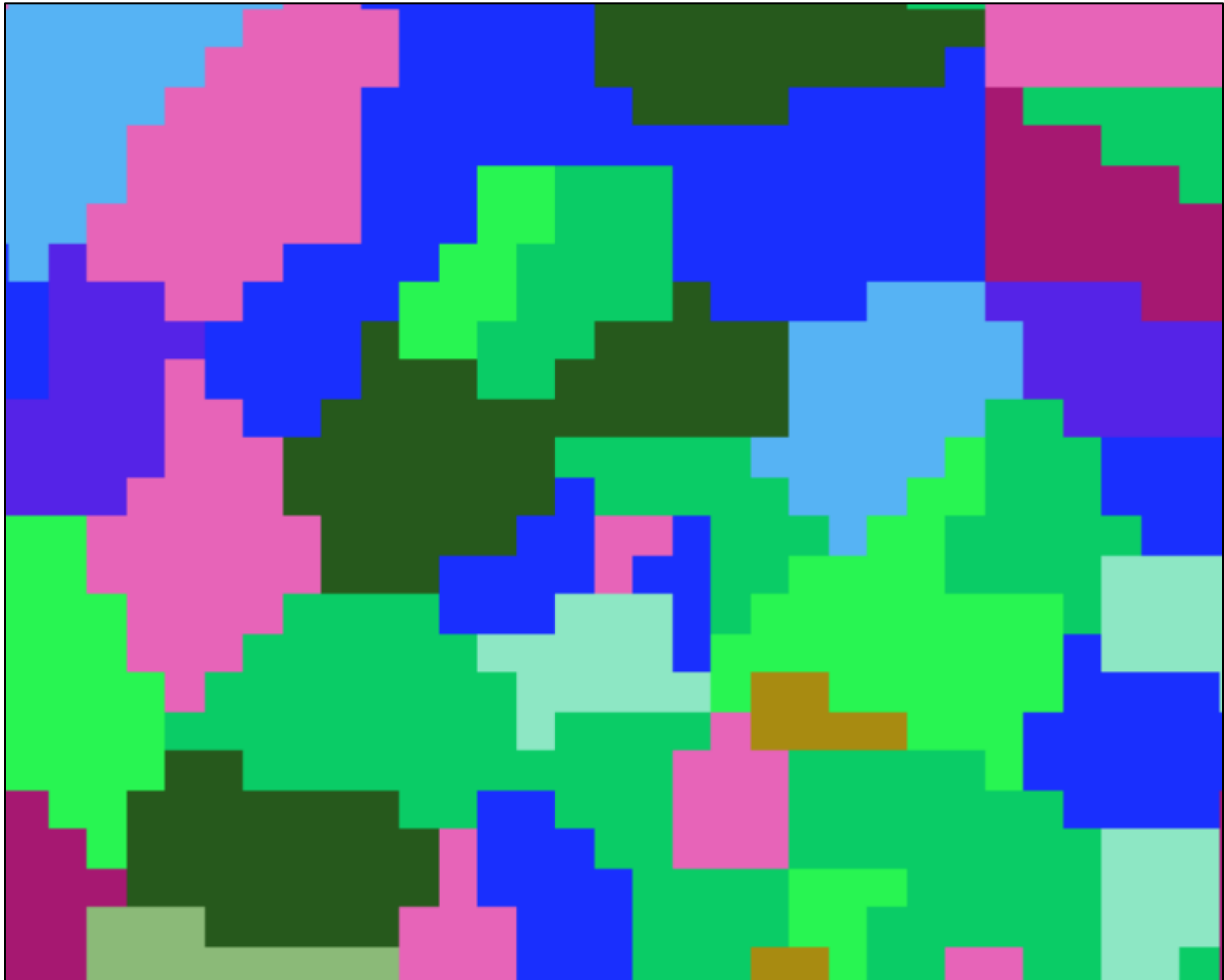


Figure A-4. Roughness Thiessen polygons converted to raster for HEC-RAS.

A.2.4 Model Simulation Range

Simulation range refers to the magnitude of flows simulated above or below the highest and lowest flows measured in the field for a particular study site. Extrapolation beyond the highest measured flow is often necessary to evaluate the possible range of flows needed by a species for activities such as juvenile rearing. The range of flow that can be simulated for a site while maintaining meaningful results is dependent on the characteristics of the transect including substrate size, hydraulic radius, bank geometry, and the presence of floodplains. Generally, to ensure extrapolated flows maintain their integrity, Physical Habitat Simulation system (PHABSIM) manuals have reported that 0.4 times the lowest flow measured to 2.5 times the highest flow measured is an acceptable simulation range (Waddle 2001), but more accurately, simulation range is limited by the channel characteristics listed above, model performance, and data availability (Waddle 2001).

Simulation range was evaluated in this study by plotting the profiles of the transects used to calibrate the models, XS-1 and XS-2, and comparing the WSELs of the simulation range needed to adequately define the area-weighted suitability (AWS) curves with the WSELs representing 0.4 times the lowest flow measured to 2.5 times the highest flow measured. The results of those WSEL comparisons are provided in Section A.3.3.

A.2.5 HEC-RAS Model Construction Methods

HEC-RAS requires the DTM be georeferenced; the horizontal location (northing and easting) and bed elevation of all the points collected from the total station were combined in a single spreadsheet tab and imported into ArcGIS Pro as a shapefile and then imported into HEC-RAS as a raster. The topographic projection of the survey points is defined in the shapefile. The shapefile is first converted to a raster using the ArcGIS geoprocessing tool Topo to Raster. The raster can then be exported from ArcGIS as a GeoTIFF. The GeoTIFF is imported into HEC-RAS as the DTM, referred to in HEC-RAS as the Terrain layer (Figure A-5). In HEC-RAS, a 2D hydraulic model is composed of a computational mesh coupled to the DTM of the bed topography. The model geometry containing the computational mesh and boundary conditions is defined once the terrain layer is in place.

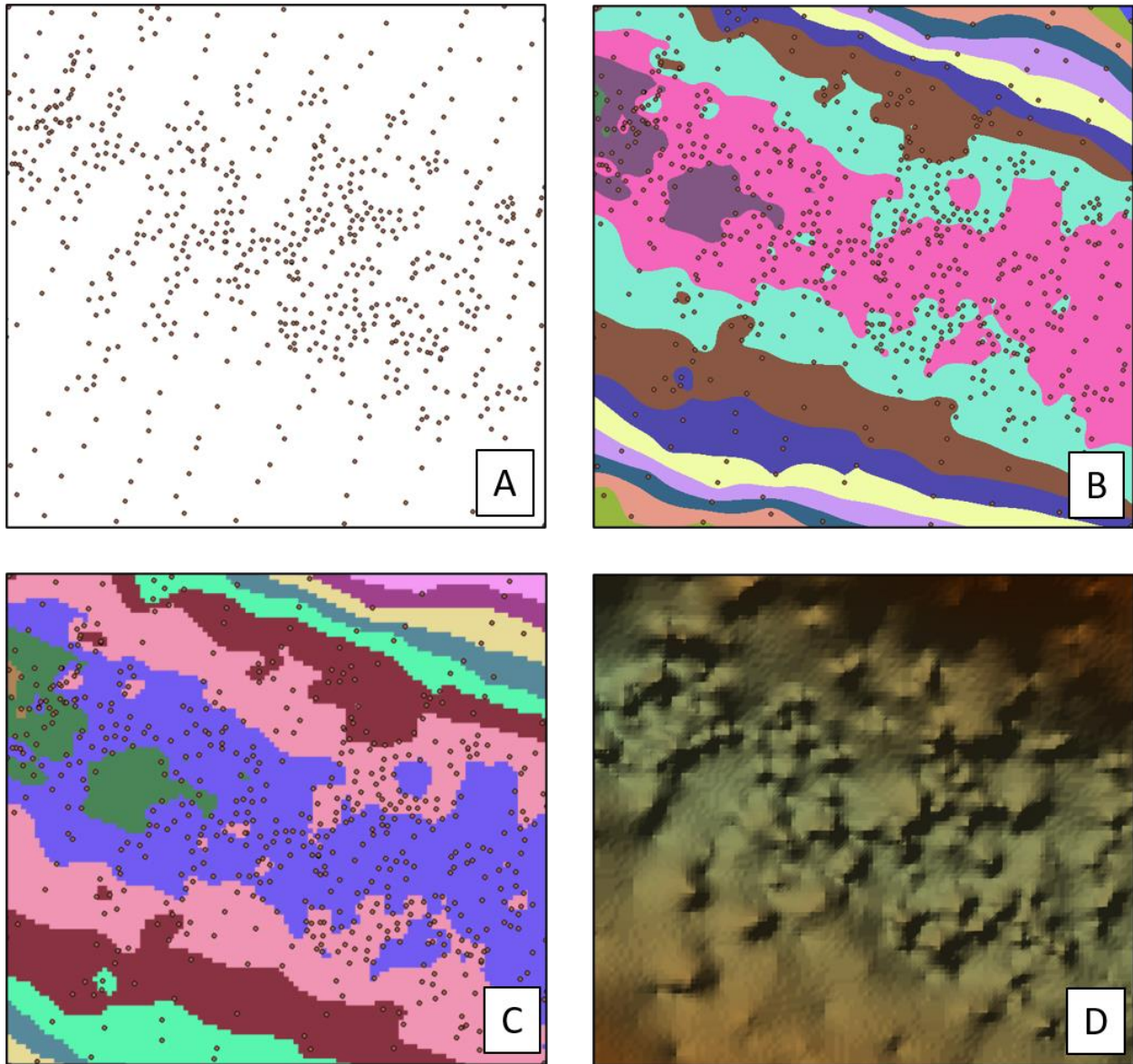


Figure A-5. Digital Terrain Model development: (A) bed topography points in ArcGIS; (B) shapefile converted to raster (Topo to Raster); (C) GeoTIFF; and (D) Terrain layer in HEC-RAS.

The first step of model development in HEC-RAS is digitizing the boundary of the 2D Flow Area within the outer boundary of the terrain layer, representing the extent of the topographic survey. Next, boundary condition lines are added to the upstream and downstream ends of the 2D Flow Area that define where flow enters and exits the model, respectively (Figure A-6). The computational mesh is first defined by adding computational points to the 2D Flow Area in a predetermined grid size, such as 1-m by 1-m or 0.5-m by 0.5-m. Ultimately, the minimum grid size is constrained by the timestep required to achieve a stable solution, refer to Section A.2.8 below. The initial grid is structured with square elements with constant mesh cell size and spacing. Cells along

the boundary of the 2D Flow Area are less structured, using a combination of triangles, squares, and rectangles to conform to the boundary shape.

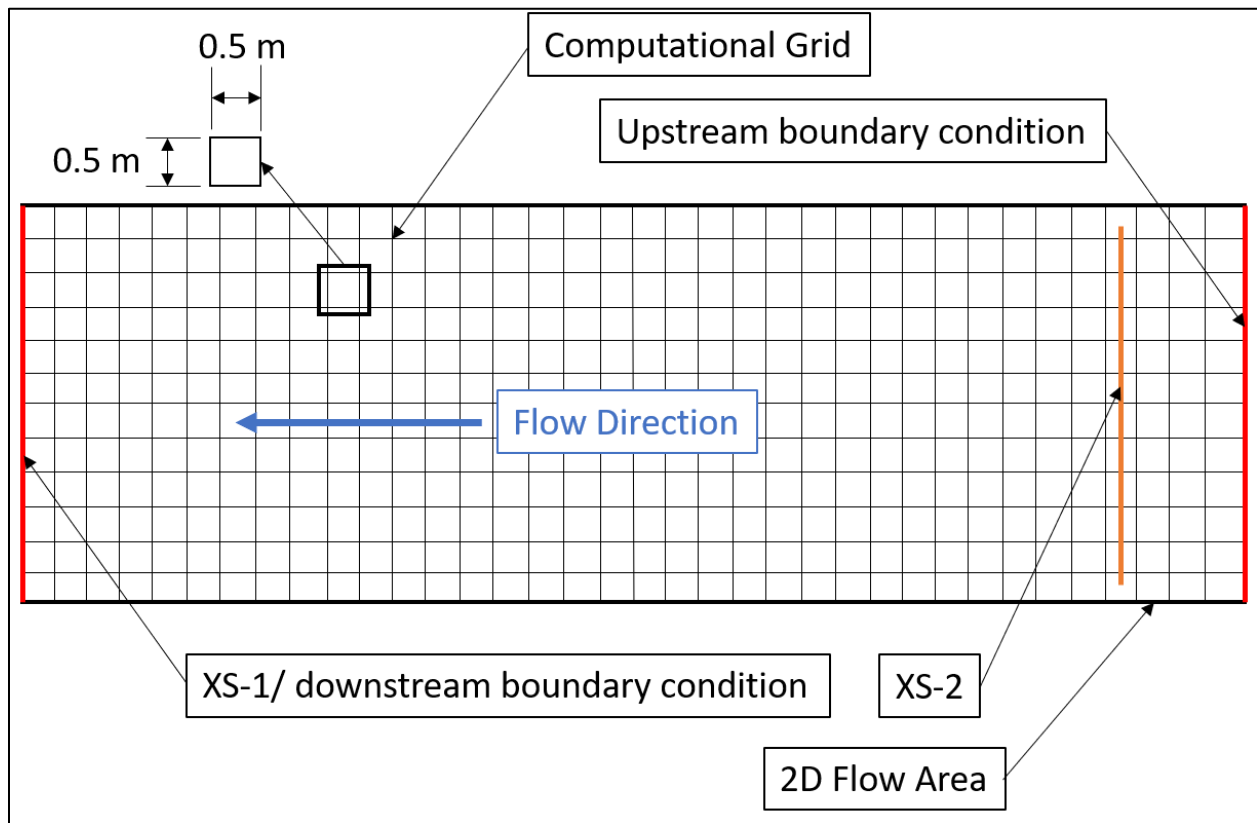


Figure A-6. HEC-RAS 2D model components.

The computational mesh in HEC-RAS is the structure used to compute depths and velocities for each grid cell shown in Figure A-6. A simplified version is provided in Figure A-7. Each cell consists of cell faces, center face points, and cell centers (Figure A-7). A single water surface is calculated at each cell center. Velocity is calculated at each cell face point and at the mid-point of each cell face. Depth is calculated across each cell face based on the resolution of the underlying terrain layer. In HEC-RAS the computational mesh and the terrain layer are decoupled. Depth is computed as the difference between the WSEL and the elevation of the underlying terrain layer. The number of depths computed across any given cell is a function of the resolution of the underlying terrain layer. This feature is referred to in HEC-RAS as sub-grid bathymetry (Figure A-8). Sub-grid bathymetry allows HEC-RAS to use larger cell sizes to express the same detailed terrain topography as if the computational grid were tied to the DTM. Model run times are reduced with larger cell sizes because fewer computations are performed in any given simulation.

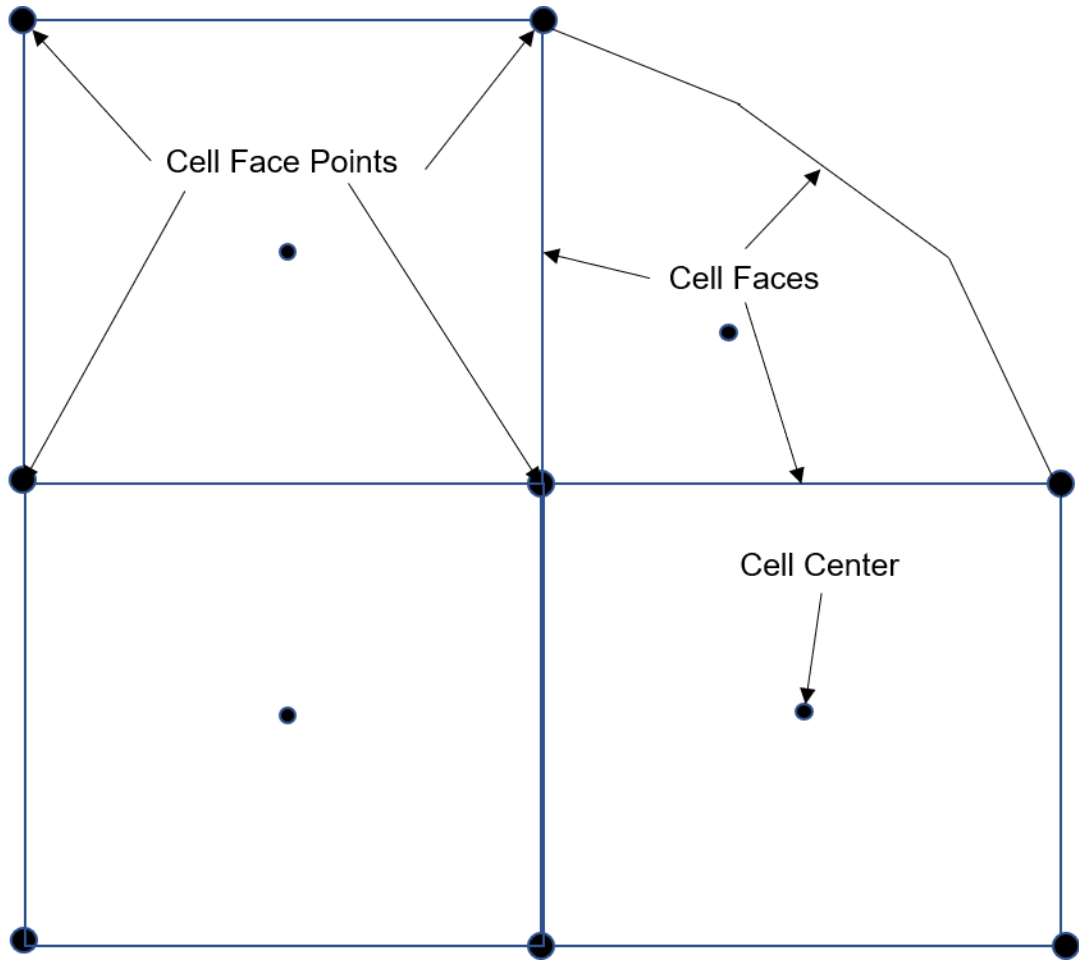


Figure A-7. Close-up view of four HEC-RAS computational grid cells including one irregular shaped boundary cell. The figure indicates which parts of the grid are cell faces, cell face points, and grid cell centers.

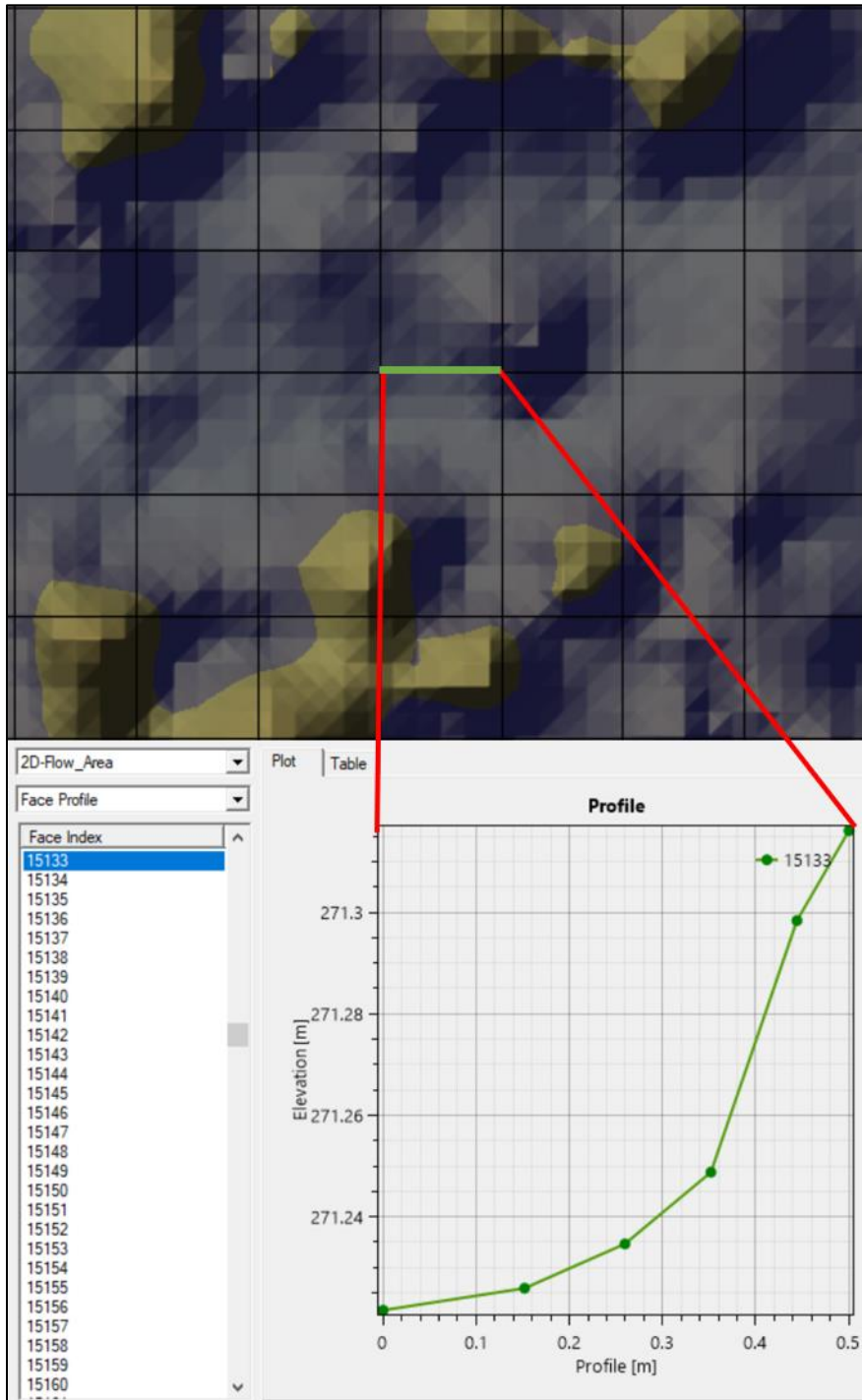


Figure A-8. HEC-RAS sub-grid bathymetry, looking down on a portion of the wetted channel from above. The green line is a flat cell face, but considers the varied terrain below shown by the elevation profile. The number 15133 is the reference for the cell face in the model.

A.2.6 HEC-RAS Model Calibration Methods

Repeated flow simulations were performed to determine that the 2D HEC-RAS model was reliably predicting the flow-WSEL relationship measured in the field. The study site boundary conditions consist of an upstream inflow boundary and downstream outflow boundary. The boundary conditions are defined in the Unsteady Flow Data menu in HEC-RAS. Although 2D HEC-RAS is an unsteady flow model, a steady state condition is achieved by assigning a single flow value in the Flow Hydrograph menu for the upstream boundary (see Figure A-6) and a constant stage value in the Stage Hydrograph menu for the downstream boundary. The downstream boundary condition is set to the XS-1 rated WSEL corresponding to the flow level being simulated. The model simulation is run until equilibrium is reached, where the downstream outflow is equal to the upstream inflow. Model performance is verified by comparing the average WSEL XS-2 at equilibrium with the XS-2 WSEL predicted by the rating relationship. Flow simulations were considered calibrated when the WSEL simulated at XS-2 was within the required tolerance of 0.1 ft (USFWS 2011) compared with the XS-2 WSEL predicted by the rating curve at the same flow level.

A.2.7 Energy Grade

HEC-RAS uses Manning's equation to solve for open channel flow in a stream channel. Manning's equation assumes uniform flow, where the stream channel bed slope equals the slope of the energy grade line (Munson et al. 1998). Normal depth is the depth at which uniform flow occurs at a given flowrate. The slope of the energy grade line is an input parameter for the Flow Hydrograph boundary condition used to define inflow at the upstream model boundary. The energy grade slope is used to estimate the normal depth of the incoming flow hydrograph given the underlying terrain data along the boundary condition line (USACE 2016). If the energy grade slope is unknown, the HEC-RAS User's Manual for Version 5.0 recommends estimating an initial value using the water surface slope or the channel bottom slope (USACE 2016).

In each study site, the upstream boundary was placed in a pool unit, where the slope of the channel bottom was not uniform. Consequently, the channel bottom slope could not be used to make an initial estimate of energy grade. A slope of 0.005 was entered for the initial flow simulation of each site. An iterative approach was used to solve for the energy grade slope. After the initial simulation, the energy grade slope was calculated using the output from the initial simulation. If the estimated energy grade slope differed from the computed value, the simulation was rerun using the computed energy grade slope until the input energy grade slope matched the output energy grade slope.

A.2.8 Diffusion Wave Approximation and Full Momentum

There are two numerical solution equations available in HEC-RAS: Diffusion Wave Approximation and Full Momentum. Both equations require the user to select an appropriate computational time step. The Courant number (CN) is used to measure whether the time step (ΔT) is short enough to capture the change in wave speed (V_s) across the mesh cell (ΔX) as follows:

$$\text{Diffusion Wave: } CN = (V_s \times \Delta T) / \Delta X \leq 2, \text{ and} \quad (\text{Equation A-4})$$

$$\text{Full Momentum: } CN = (V_s \times \Delta T) / \Delta X \leq 1. \quad (\text{Equation A-5})$$

The numerical thresholds are suggested for each equation type (WEST Consultants Inc 2017). Practically, the smallest allowable cell size of the mesh is limited by the maximum expected speed of water moving through a cell. Diffusion Wave Approximation (DWA) has faster run times and is inherently more stable than Full Momentum (FM), but DWA is limited in application. DWA is a good choice when the fluid dynamics can be simplified to the assumptions of Manning's equation. DWA is good with gradually varying flows with moderate to steep slopes. DWA does not appropriately simulate flow separations, eddies, or main channel/overbank momentum transfers. Full Momentum should be used with highly dynamic flood waves such as flash flood/dam breach, sudden hydraulic expansion or contraction, tidal conditions, wave run-up, super elevation around bends, detailed velocities and stages at structures, mixed flow regime simulations, and main channel to overbank momentum transfers (WEST Consultants Inc 2017).

In this study, DWA was used to determine initial n values, check energy gradient (EG) and Froude number (FN), and estimate the run-time necessary to achieve flow equilibrium across the site. All flow simulations were performed using FM to determine if a stable solution could be achieved. Stable solutions required the final outflow to be within 1% of the inflow and the final outflow hydrograph to be a constant magnitude using a timestep of 0.1 seconds, the shortest computational timestep available in HEC-RAS. DWA was used for simulations if the final outflow, using FM, was not within 1% of the inflow or if the outflow was not a constant magnitude.

After each simulation was completed, CN and FN were reviewed in the RAS-Mapper for each computational mesh cell. Values were checked to see whether the CN exceeded 2.0 for DWA or 1.0 for FM. The RAS-Mapper visual display color scale was set to a threshold value to facilitate output data verification.

FN is a dimensionless parameter that describes the relationship between water velocity and wave speed. When FN reaches 1.0, the water velocity exceeds the wave speed, and upstream traveling waves are washed downstream (Munson et al. 1998). At FN =

1.0, flow transitions from laminar, subcritical flow to critical flow, and as FN becomes greater than 1.0, to supercritical flow. Supercritical conditions are characterized by turbulent flow, the onset of vertical mixing, a break in hydraulic slope continuity or a hydraulic jump (Munson et al. 1998). Although HEC-RAS is capable of solving water depth and velocity in critical to supercritical flow conditions, depths and velocities estimated from a 2D model in subcritical, ideally laminar flow (FN <1.0), are more reliable.

A.2.9 HEC-RAS Depth and Velocity Validation Methods

Depth and velocity validation are the final step after the 2D model is calibrated and simulations have been completed over the flow range required for the fish habitat evaluation. Water depths and velocities were measured in the field at random locations within each study site, refer to Section 3.3 of the main report for details about data collection methodology. The exact location and stream bed elevation were recorded with the total station. A minimum of 50 validation measurements were recorded for each site (USFWS 2011). A discharge measurement was taken before the validation depth and velocity measurements were recorded. A 2D model simulation was then completed at the flow recorded in the field. The field depth and velocity measurements were compared to the depths and velocities predicted by the 2D model at the same locations and at the same flow level.

Validation data results were viewed by plotting the field-measured value versus the simulated value for each point, depth, and velocity. The correlation coefficient (R^2) of the depth measurements should be greater than or equal to 0.9, and the velocities are expected to have a correlation coefficient of at least 0.6 (USFWS 2011).

A.3 Model Calibration and Validation Results

Section A.3 provides the results of the flow-WSEL calibration used to simulate flows, the RM's used to calibrate the flow simulations, simulation flow ranges used to adequately define the AWS curve for each study site, XS-2 WSEL calibration, hydraulic parameters monitored during each simulation, and the depth and velocity validation results.

A.3.1 Flow-WSEL Calibration Results

This section of the appendix provides the flow-WSEL rating relationships for each study site. Rating curve data consisting of discharge, WSEL, and SZF measurements were collected using tape, wading rod, velocity meter, auto-level, and stadia rods in imperial units. Vertical control for the differential leveling surveys was maintained by establishing

vertical benchmarks (VBM) composed of lag bolts in tree trunks near each transect. The VBMs were assigned a local coordinate height of 100 ft for the differential leveling surveys. Each VBM was then surveyed with the total station so that the WSELs and SZFs could be converted into the North American Vertical Datum of 1988 (NAVD 88), the vertical datum used in the HEC-RAS model (Table A-3). Table A-4 through Table A-9 provide the flow-WSEL data used to create the ratings. Figure A-9 through Figure A-14 present the flow-WSEL data and the best-fit log-log regressions used to predict WSEL over the range of flows needed to meet the study objectives. Table A-4 through Table A-9 and Figure A-9 through Figure A-14 are ordered by site and transect number, from Site 1, XS-1 to Site 3, XS-2, respectively. The goodness of fit of each rating regression was measured using R^2 . The R^2 was computed for each rating with a minimum of 0.9918 at Site 2, XS-1.

Table A-3. XS survey control data.

Site	XS	VBM (m)	SZF (m)
1	1	209.810	208.533
1	2	212.825	211.818
2	1	271.522	270.217
2	2	275.692	274.854
3	1	310.251	309.288
3	2	313.026	311.718

Table A-4. Site 1: XS-1 flow-WSEL data.

Date	Q (cfs)	Q (cms)	WSEL (m)	LOG (Q)	LOG (WSEL-SZF)
4/24/2018	3.2	0.091	208.777	-1.043	-0.613
5/16/2018	1.2	0.034	208.722	-1.469	-0.724
1/10/2019	29.2	0.827	209.002	-0.083	-0.328
1/11/2019	13.8	0.391	208.917	-0.408	-0.416

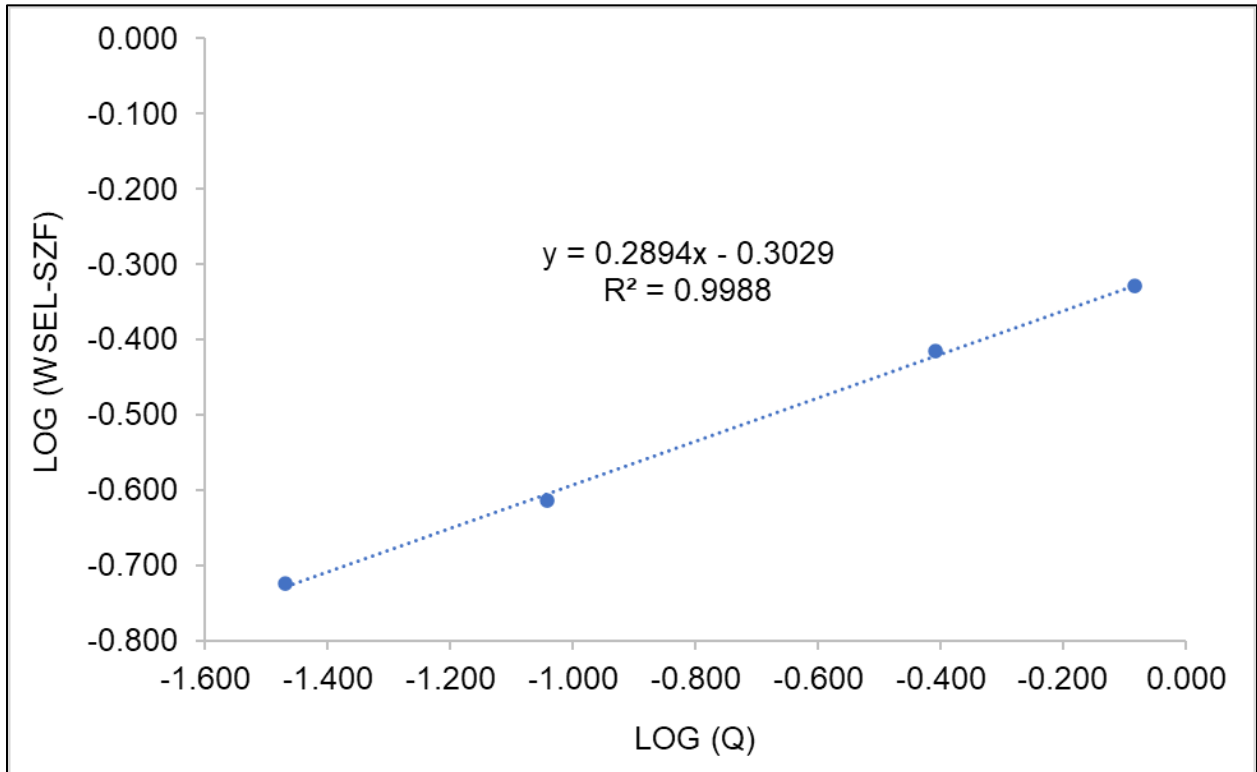


Figure A-9. Site 1: XS-1 log-log regression.

Table A-5. Site 1: XS-2 flow-WSEL data.

Date	Q (cfs)	Q (cms)	WSEL (m)	LOG (Q)	LOG (WSEL-SZF)
4/24/2018	3.2	0.091	211.959	-1.043	-0.850
5/16/2018	1.2	0.034	211.917	-1.469	-1.006
1/10/2019	29.2	0.827	212.164	-0.083	-0.461
1/11/2019	13.8	0.391	212.078	-0.408	-0.585

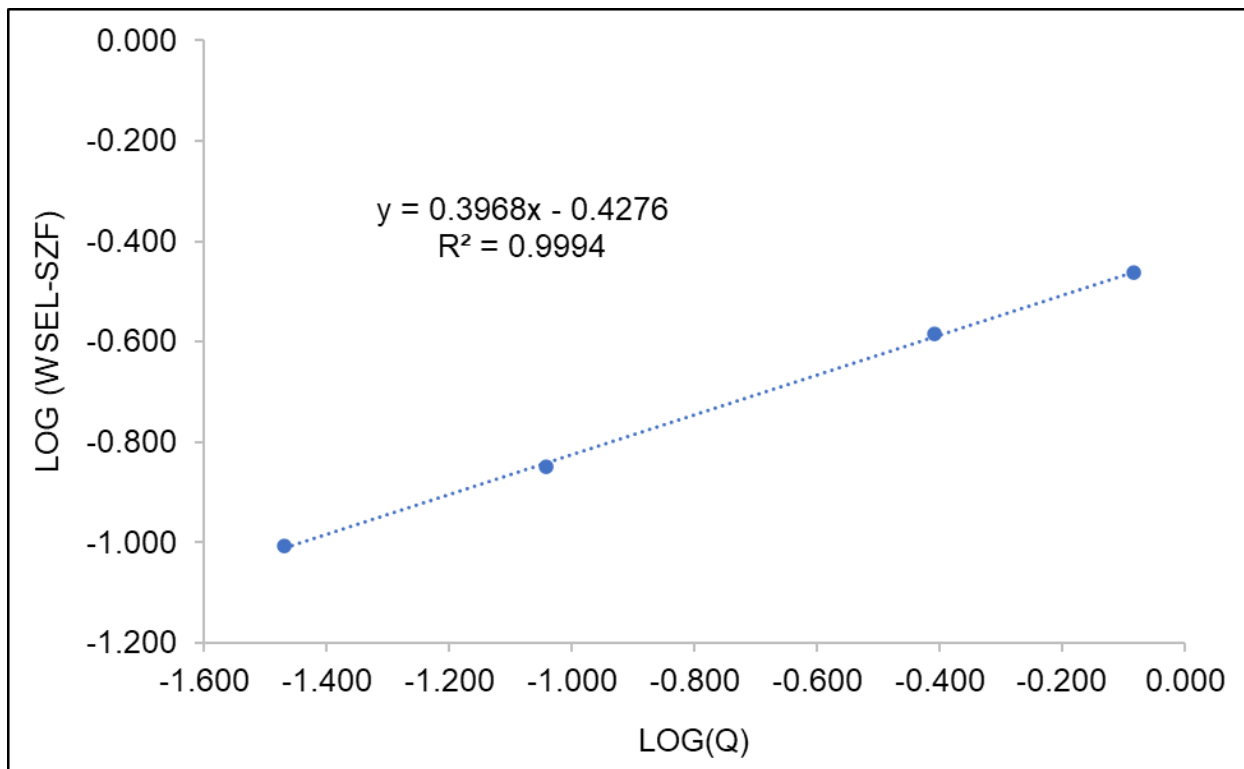


Figure A-10. Site 1: XS-2 log-log regression.

Table A-6. Site 2: XS-1 flow-WSEL data.

Date	Q (cfs)	Q (cms)	WSEL (m)	LOG (Q)	LOG (WSEL-SZF)
4/16/2018	5.3	0.150	270.352	-0.824	-0.873
4/18/2018	3.7	0.105	270.327	-0.980	-0.960
4/25/2018	1.6	0.045	270.297	-1.344	-1.101
5/16/2018	0.8	0.023	270.281	-1.645	-1.194
1/11/2019	10.5	0.297	270.409	-0.527	-0.718
1/18/2019	26.3	0.744	270.495	-0.128	-0.557
1/31/2019	2.2	0.062	270.306	-1.206	-1.053

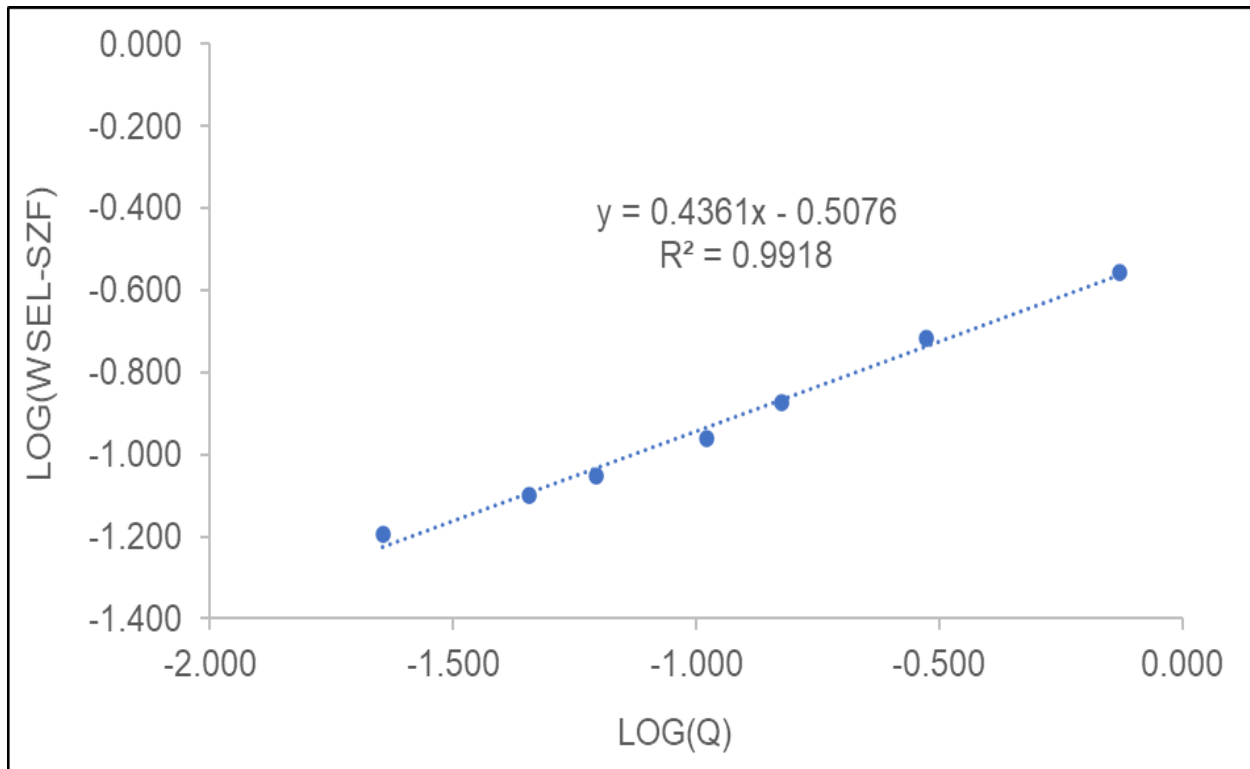


Figure A-11. Site 2: XS-1 log-log regression.

Table A-7. Site 2: XS-2 flow-WSEL data.

Date	Q (cfs)	Q (cms)	WSEL (m)	LOG (Q)	LOG (WSEL-SZF)
4/16/2018	5.3	0.150	275.131	-0.824	-0.557
4/18/2018	3.7	0.105	275.107	-0.980	-0.597
4/25/2018	1.6	0.045	275.061	-1.344	-0.683
5/16/2018	0.8	0.023	275.021	-1.645	-0.776
1/11/2019	10.5	0.297	275.180	-0.527	-0.487
1/18/2019	26.3	0.744	275.281	-0.128	-0.370
1/31//2019	2.2	0.062	275.076	-1.206	-0.653

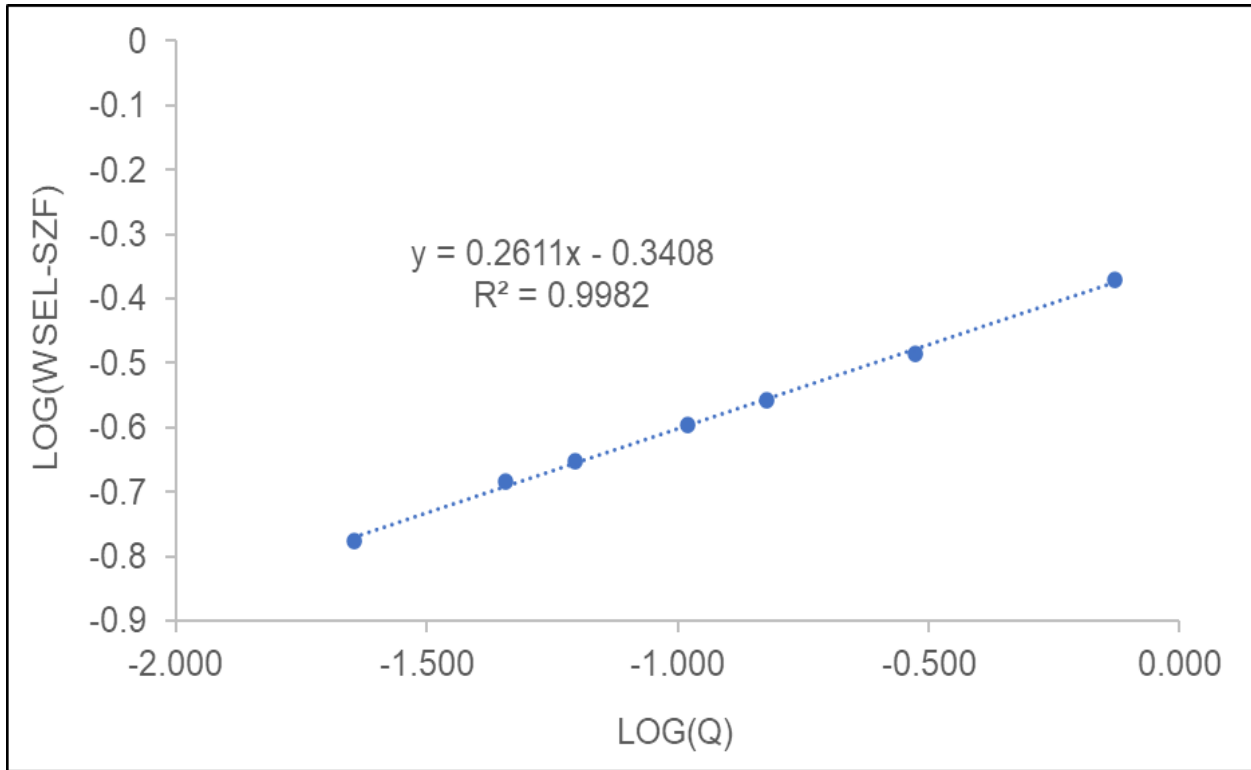


Figure A-12. Site 2: XS-2 log-log regression.

Table A-8. Site 3: XS-1 flow-WSEL data.

Date	Q (cfs)	Q (cms)	WSEL (m)	LOG (Q)	LOG (WSEL-SZF)
3/14/2019	8.1	0.229	309.696	-0.639	-0.389
4/24/2019	2.0	0.057	309.571	-1.247	-0.548
6/4/2019	1.0	0.028	309.523	-1.548	-0.629

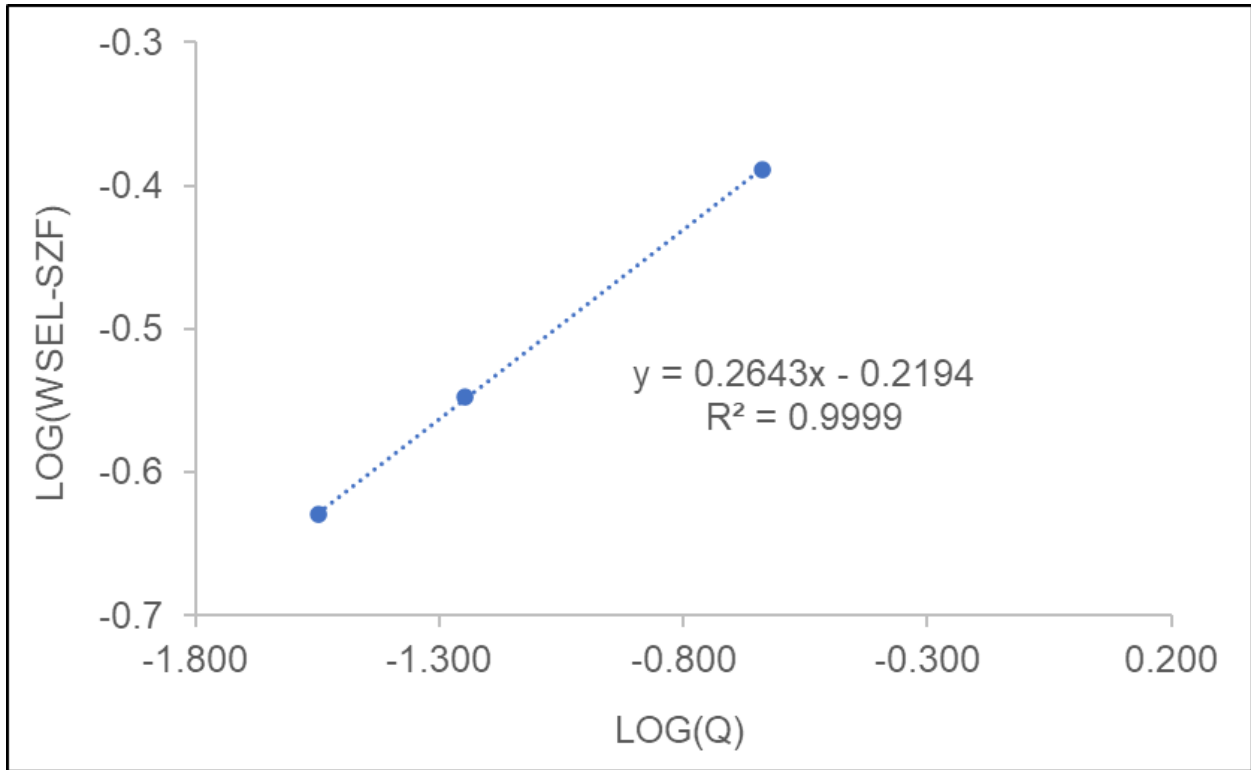


Figure A-13. Site 3: XS-1 log-log regression.

Table A-9. Site 3: XS-2 flow-WSEL data.

Date	Q (cfs)	Q (cms)	WSEL (m)	LOG (Q)	LOG (WSEL-SZF)
3/14/2019	8.1	0.229	311.920	-0.639	-0.696
4/24/2019	2.0	0.057	311.822	-1.247	-0.983
6/4/2019	1.0	0.028	311.795	-1.548	-1.116

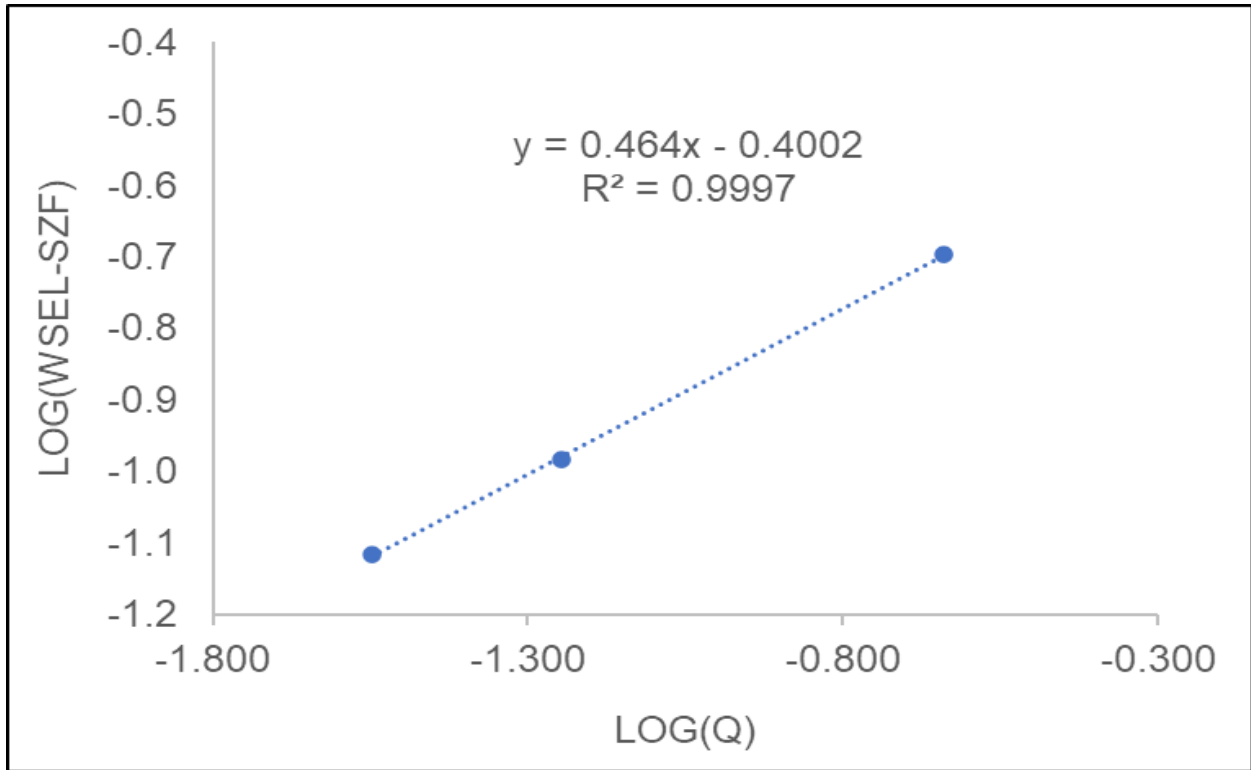


Figure A-14. Site 3: XS-2 log-log regression.

A.3.2 Stream Channel Roughness Results

A simulation was executed for each site using the unfactored stream channel roughness map imported into HEC-RAS from ArcGIS (RM = 1.0). The initial flow simulation run for each site was the highest target flow level for that site as follows: 40 cfs in Site 1, 30 cfs in Site 2, and 20 cfs in Site 3. Table A-10 gives the range of n values produced by these unfactored roughness maps. None of the initial simulations calibrated; the average simulated WSELs at XS-2 were less than the rating WSEL by more than the guidance threshold of 0.1 ft.

Table A-10. Initial simulation roughness.

Site	Flow Simulation (cfs)	Median Substrate Size (ft)	Manning's <i>n</i> Range	Mean Manning's <i>n</i>	Median Manning's <i>n</i>
1	40	0.33	0.020–0.048	0.037	0.039
2	30	0.58	0.020–0.048	0.039	0.044
3	20	>1.0	0.020–0.048	0.042	0.048

To calibrate the flow simulations, the values for each roughness map were multiplied by a constant RM. Simulations were executed across the flow range of each site to adequately define the AWS curve (Table A-11). Different ranges of flow and increments of flow were required to identify the peak AWS value for each site.

Table A-11. Calibrated model roughness values.

Site	Flow Simulations (cfs)	RM	Manning's <i>n</i> Range	Mean Manning's <i>n</i>	Median Manning's <i>n</i>
1	10, 15, 20, 24.3, 30, 35, 40, 45, 50, 60, & 70	2.125	0.043–0.102	0.078	0.084
1	1, 2, 3, 4, 4.5, & 5	3.0	0.061–0.144	0.110	0.118
2	1, 2, 2.2, 2.4, 3, 4, 5, 10, 10.5, 15, 20, 25, 30, 35, 40, 50, 60, & 70	1.5	0.031–0.072	0.058	0.065
3	1, 2, 3, 4, 5, 10, 15, 17, 18, 19, 20, 21, 22, 25, 30, 40, & 50	1.25	0.025–0.060	0.053	0.060

Site 1 required two different RMs to calibrate the flows over the entire simulation range. Sites 2 and 3 were calibrated over the full simulation range using a constant RM, 1.5 for Site 2 and 1.25 for Site 3.

A.3.3 Simulation Range Results

The purpose of the hydraulic modeling was to simulate flows over a range that defined the shape of the AWS curve for each site. Table A-12 reports the highest and lowest flows sampled at each site, 0.4 times the lowest flow sampled, 2.5 times the highest

flow sampled, and the highest and lowest simulated flows used to define the AWS curve for each site.

Table A-12. Sampled flow range and simulated flow range results.

Site	Condition	Flows (cfs)	Factor
1	lowest flow sampled	1.2	1.0
1	highest flow sampled	29.2	1.0
1	0.4 x lowest flow sampled	0.5	0.4
1	2.5 x highest flow sampled	73.0	2.5
1	lowest flow simulated	1.0	1.0
1	highest flow simulated	70.0	2.4
2	lowest flow sampled	0.8	1.0
2	highest flow sampled	26.3	1.0
2	0.4 x lowest flow sampled	0.3	0.4
2	2.5 x highest flow sampled	65.7	2.5
2	lowest flow simulated	1.0	1.0
2	highest flow simulated	70.0	2.7
3	lowest flow sampled	1.0	1.0
3	highest flow sampled	8.1	1.0
3	0.4 x lowest flow sampled	0.4	0.4
3	2.5 x highest flow sampled	20.3	2.5
3	lowest flow simulated	1.0	1.0
3	highest flow simulated	50.0	6.2

The lowest flows simulated were equal to or greater than 0.4 times the lowest flow sampled. The highest flow simulated for Site 1 was 2.4 times the highest flow sampled and for Site 2 was 2.7 times the highest flow sampled, slightly more than the suggested upper limit of 2.5. Plots of the difference in WSEL between 2.5 and 2.7 times the highest flow sampled were imperceptible. The highest flow simulated for Site 3, 50 cfs, was 6.2 times the highest flow sampled. The average WSELs corresponding to the range of flows simulated in Site 3 are plotted in Figure A-15 for XS-1 and Figure A-16 for XS-2 as follows: the lowest flow sampled and simulated, 1.0 cfs, 2.5 times the highest flow

sampled, 20.3 cfs, and the highest flow simulated, 50 cfs. Fieldwork to measure WSELs and flows for greater than 8.1 cfs for Site 3 was not possible due to COVID19 fieldwork restrictions.

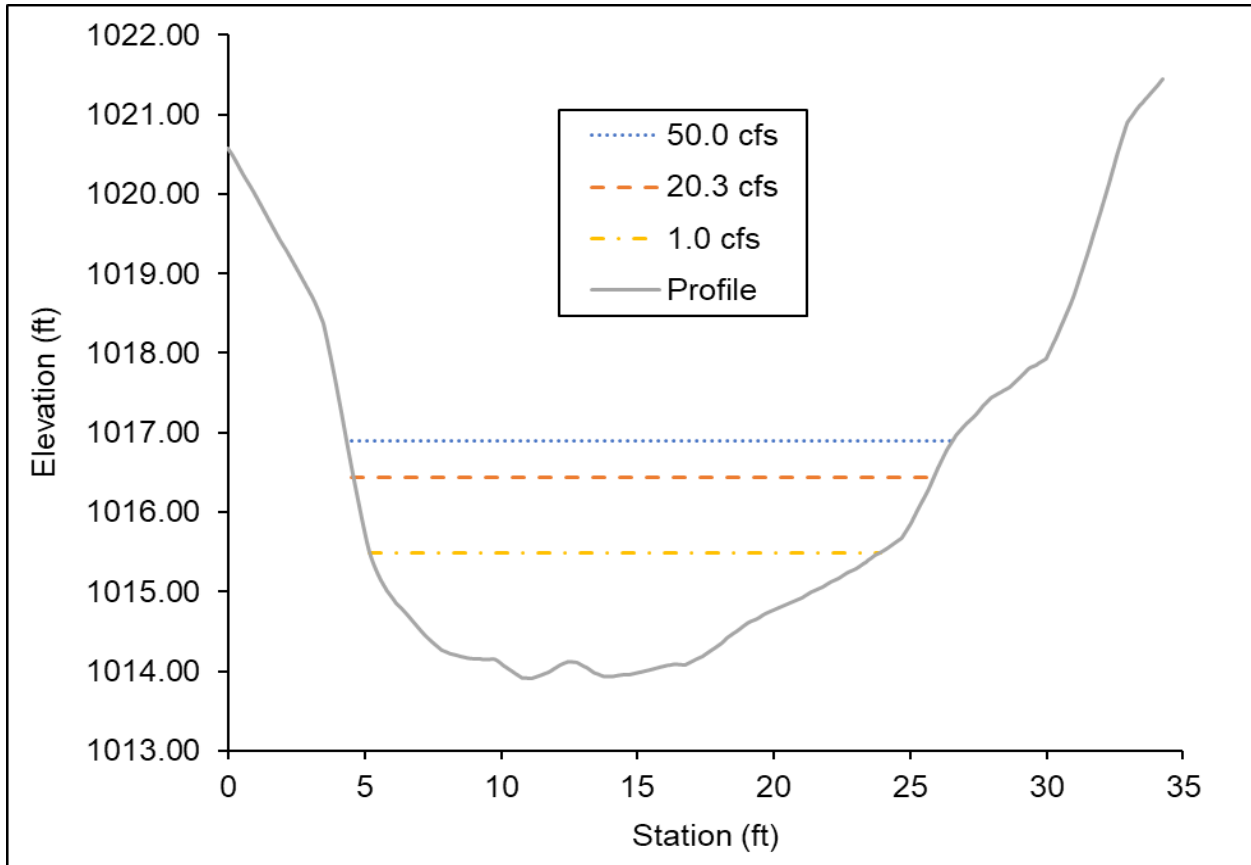


Figure A-15. Site 3, XS-1 flow simulation range.

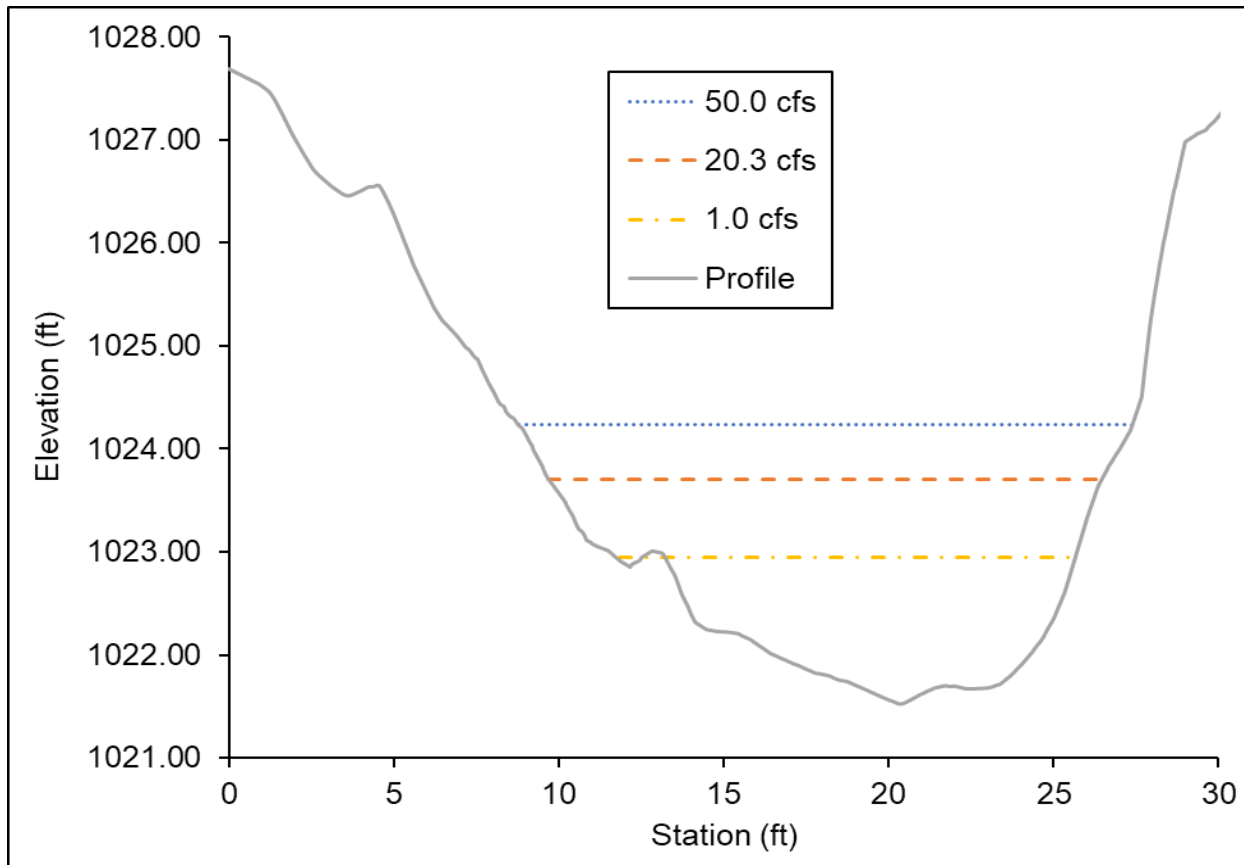


Figure A-16. Site 3, XS-2 flow simulation range.

The average simulated Site 3 WSEL at 50 cfs plots along a constant bank slope in relation to 20.3 cfs in XS-1. There is a slight change in the slope of the right bank of XS-2 between 20.3 cfs and 50 cfs. The highest simulated flow of 50 cfs is still well within the banks of XS-2. The bank slope geometry of Site 3 appears to support expanding the upper simulation limit to 6.2 times the highest measured flow.

A.3.4 HEC-RAS WSEL Calibration Results

Table A-13 through Table A-15 provide the WSEL calibration results for Sites 1, 2, and 3, respectively. Using the RM values in Table A-11, all of the simulations for the three sites were below the 0.1 ft threshold for the difference between the rating WSEL and simulated average WSEL at XS-2.

Table A-13. Site 1 WSEL simulation calibration results.

Site Discharge (cfs)	Rating XS-2 WSEL (ft)	Simulated XS-2 WSEL (ft)	(+/-) (ft)
70	696.55	696.64	0.09
60	696.45	696.51	0.06
50	696.35	696.38	0.03
45	696.29	696.31	0.02
40	696.23	696.23	0.00
35	696.16	696.15	-0.01
30	696.09	696.06	-0.03
24.3	696.00	695.95	-0.05
20	695.92	695.86	-0.06
15	695.81	695.74	-0.08
10	695.68	695.59	-0.09
5	695.51	695.49	-0.01
4.5	695.48	695.46	-0.02
4	695.46	695.43	-0.02
3	695.40	695.37	-0.03
2	695.33	695.29	-0.05
1	695.24	695.18	-0.06

Table A-14. Site 2 WSEL simulation calibration results.

Site Discharge (cfs)	Rating XS-2 WSEL (ft)	Simulated XS-2 WSEL (ft)	(+/-) (ft)
70	903.54	903.63	0.09
60	903.47	903.54	0.07
50	903.39	903.44	0.05
40	903.30	903.33	0.03
35	903.24	903.26	0.02
30	903.19	903.19	0.00
25	903.12	903.12	0.00
20	903.04	903.03	-0.01
15	902.95	902.93	-0.02
10.5	902.84	902.81	-0.03
10	902.83	902.79	-0.04
5	902.65	902.61	-0.04
4	902.60	902.55	-0.05
3	902.54	902.50	-0.04
2.4	902.50	902.46	-0.04
2.2	902.48	902.44	-0.04
2	902.46	902.43	-0.03
1	902.34	902.33	-0.01

Table A-15. Site 3 WSEL simulation calibration results.

Site Discharge (cfs)	Rating XS-2 WSEL (ft)	Simulated XS-2 WSEL (ft)	(+/-) (ft)
50	1024.23	1024.14	-0.09
40	1024.08	1024.01	-0.07
30	1023.91	1023.86	-0.05
25	1023.81	1023.76	-0.05
22	1023.75	1023.70	-0.05
21	1023.72	1023.68	-0.04
20	1023.70	1023.65	-0.05
19	1023.68	1023.64	-0.04
18	1023.65	1023.61	-0.04
17	1023.63	1023.59	-0.04
15	1023.57	1023.54	-0.03
10	1023.42	1023.41	-0.01
5	1023.22	1023.24	0.02
4	1023.17	1023.20	0.03
3	1023.11	1023.15	0.04
2	1023.04	1023.09	0.05
1	1022.95	1023.00	0.05

A.3.5 HEC-RAS 2D Hydraulic Solution Results

All the flow simulations summarized in Table A-11 were executed using the FM equation set. All of the FM simulations in Sites 1, 2, and 3 reached equilibrium with less than 1% difference in net flow, inflow versus outflow. However, there was a marked difference between the flow FM simulations executed for Site 1 than for Sites 2 and 3. As indicated in Table A-11, flow simulations for Sites 2 and 3 were completed using a composite roughness raster based upon substrate coding and a single RM, 1.5 for Site 2 and 1.25 for Site 3. The initial FM simulations in Site 1 required four separate RMs (Table A-16). Ideally, when using a composite raster to express bed roughness spatially within each site, only a single RM should be needed to calibrate flow-WSEL. While FM

can be more precise, DWA is inherently more stable and efficient from a run time perspective. The Site 1 simulations were rerun using DWA. As indicated in Table A-11, only two RMs were required to calibrate flows simulated from 1 to 70 cfs, with the break occurring between 5 and 10 cfs.

Table A-16. Site 1 Bed Roughness Multipliers when using the FM equation set.

Simulated Flow (cfs)	FM/RM
40, 45, 50, 60, & 70	1.5
20, 24.3, 30, & 35	2.0
15	2.5
1, 2, 3, 4, 4.5, 5, & 10	3.0

As described in Section A.2.7, an EG slope of 0.005 was entered into the initial simulation for each site. An iterative approach was used to adjust the EG slope. After each simulation, the water surface in the upstream boundary condition pool unit was computed and the EG slope was adjusted as necessary for each subsequent simulation. EG slopes in the upstream boundary pool ranged from 0.004 in the highest flow simulations to 0.000 in the lower flow simulations (Table A-17).

Table A-17. EG slope range.

Site	High Flow (cfs)	EG	Low Flow (cfs)	EG
1	70	0.005	1	0.000
2	70	0.004	1	0.000
3	50	0.002	1	0.001

After WSEL calibration was completed for each simulation, the remaining simulation threshold parameters were generated for Sites 1, 2, and 3 and are presented in Table A-18, Table A-19, and Table A-20, respectively. Net flow refers to the difference between the flow hydrograph defined at the upstream boundary and the final value of the flow output hydrograph reported for the downstream boundary at the end of the simulation. CN and FN were exported from HEC-RAS into ArcGIS as TIFFs for each flow simulation and computational mesh cell.

Table A-18. Site 1 HEC-RAS model DWA flow simulation parameters.

Flow (cfs)	Final Simulation Flow (cfs)	Net Flow	Maximum CN	Average FN	Maximum FN
70	70.0	0.00%	1.21	0.30	4.27
60	60.0	0.00%	1.13	0.29	5.60
50	50.0	0.00%	1.04	0.28	4.67
45	45.0	0.00%	0.98	0.28	4.02
40	40.0	0.00%	0.92	0.27	5.64
35	35.0	0.00%	0.86	0.26	6.62
30	30.0	0.00%	0.79	0.25	6.96
24.3	24.3	0.00%	0.71	0.24	6.38
20	20.0	0.00%	0.64	0.23	5.47
15	15.0	0.00%	0.63	0.21	4.49
10	10.0	0.00%	0.92	0.19	5.52
5	5.0	0.00%	0.63	0.19	3.32
4.5	4.5	0.00%	0.62	0.11	3.89
4	4.0	0.00%	0.45	0.11	2.81
3	3.0	0.00%	0.42	0.10	3.52
2	2.0	0.00%	0.37	0.09	3.43
1	1.0	0.00%	0.48	0.07	2.71

Table A-19. Site 2 HEC-RAS model FM flow simulation parameters.

Flow (cfs)	Final Simulation Flow (cfs)	Net Flow	Maximum CN	Average FN	Maximum FN
70	70.0	0.00%	0.75	0.41	12.63
60	60.0	0.00%	0.74	0.40	11.80
50	50.0	0.00%	0.71	0.39	8.31
40	40.0	0.00%	0.69	0.37	8.28
35	35.0	0.00%	0.67	0.36	9.88
30	30.0	0.00%	0.65	0.35	8.49
25	25.0	0.00%	0.63	0.34	9.05
20	20.0	0.00%	0.90	0.32	9.04
15	15.0	0.00%	0.85	0.30	7.19
10.5	10.5	0.00%	0.78	0.27	6.96
10	10.0	0.00%	0.77	0.27	5.89
5	5.0	0.00%	0.65	0.23	8.01
4	4.0	0.00%	0.87	0.22	7.01
3	3.0	0.00%	0.66	0.20	6.66
2.4	2.4	0.00%	0.64	0.19	6.58
2.2	2.2	0.00%	0.63	0.18	5.25
2	2.0	0.00%	0.63	0.18	7.17
1	1.0	0.00%	0.76	0.14	4.74

Table A-20. Site 3 HEC-RAS model FM flow simulation parameters.

Flow (cfs)	Final Simulation Flow (cfs)	Net Flow	Maximum CN	Average FN	Maximum FN
50	50.0	0.00%	0.51	0.41	10.32
40	40.0	0.00%	0.93	0.39	11.96
30	30.0	0.00%	0.89	0.37	14.12
25	25.0	0.00%	0.87	0.35	12.62
22	22.0	0.00%	0.86	0.34	13.73
21	21.0	0.00%	0.85	0.34	9.27
20	20.0	0.00%	0.84	0.33	10.52
19	19.0	0.00%	0.84	0.33	8.96
18	18.0	0.00%	0.83	0.33	7.65
17	17.0	0.00%	0.82	0.32	15.81
15	15.0	0.00%	0.81	0.31	12.22
10	10.0	0.00%	0.74	0.28	8.60
5	5.0	0.00%	0.94	0.23	8.55
4	4.0	0.00%	0.60	0.22	11.91
3	3.0	0.00%	0.57	0.20	11.56
2	2.0	0.00%	0.53	0.18	5.87
1	1.0	0.00%	0.68	0.14	5.73

The CN values for the DWA simulations of Site 1 were all below the 2.0 threshold (Table A-18) and in Sites 2 and 3 the CN values for the FM solutions were all below the 1.0 threshold (Table A-19 and Table A-20).

FN was evaluated in each simulation; the maximum FN for an individual cell exceeded 1.0 in all the simulations. FN values were below 1.0 in shallow wetted areas where juvenile salmonids are expected to rear. Computational mesh cells with FNs >1.0 were only observed around the perimeters of substrate protruding above the water surface and sporadically along the wetted stream margins. The flow simulation with the largest peak FN value and the area in each site with the concentration of highest FNs values are plotted below in Figure A-17, Figure A-18, and Figure A-19 for Sites 1, 2, and 3, respectively.

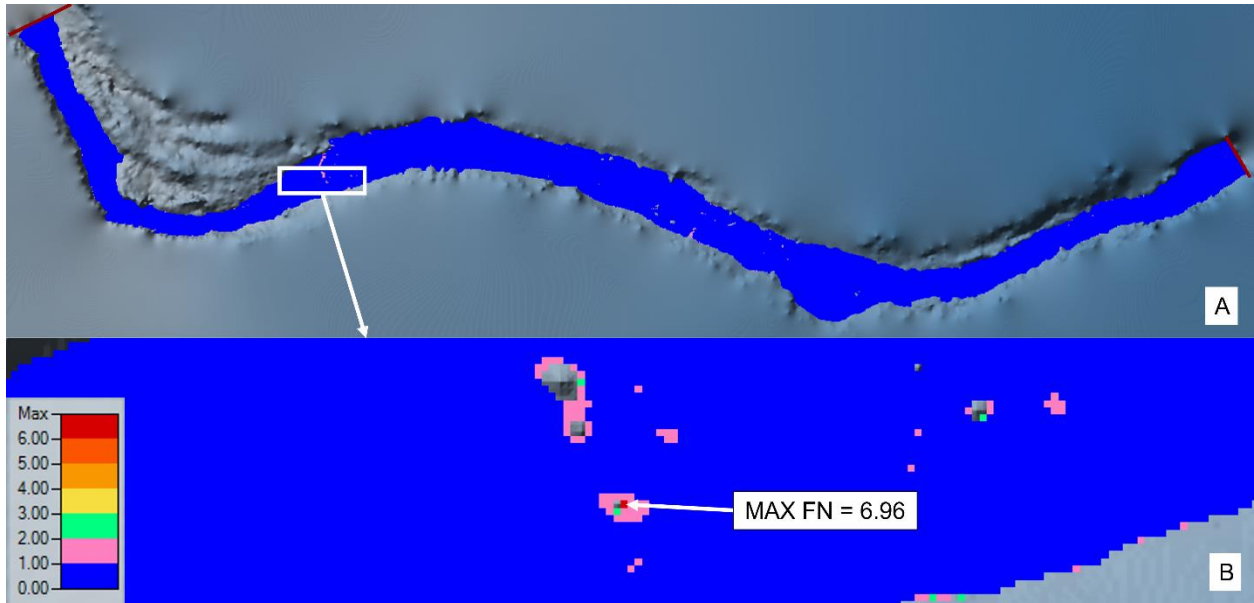


Figure A-17. (A) Site 1 FN display at 30 cfs. Blue cells are FN <1.0, purple, green, and red cells appear sporadically near bed, bank, and substrate boundaries where FN >1.0. (B) Zoomed in on cell with max FN.

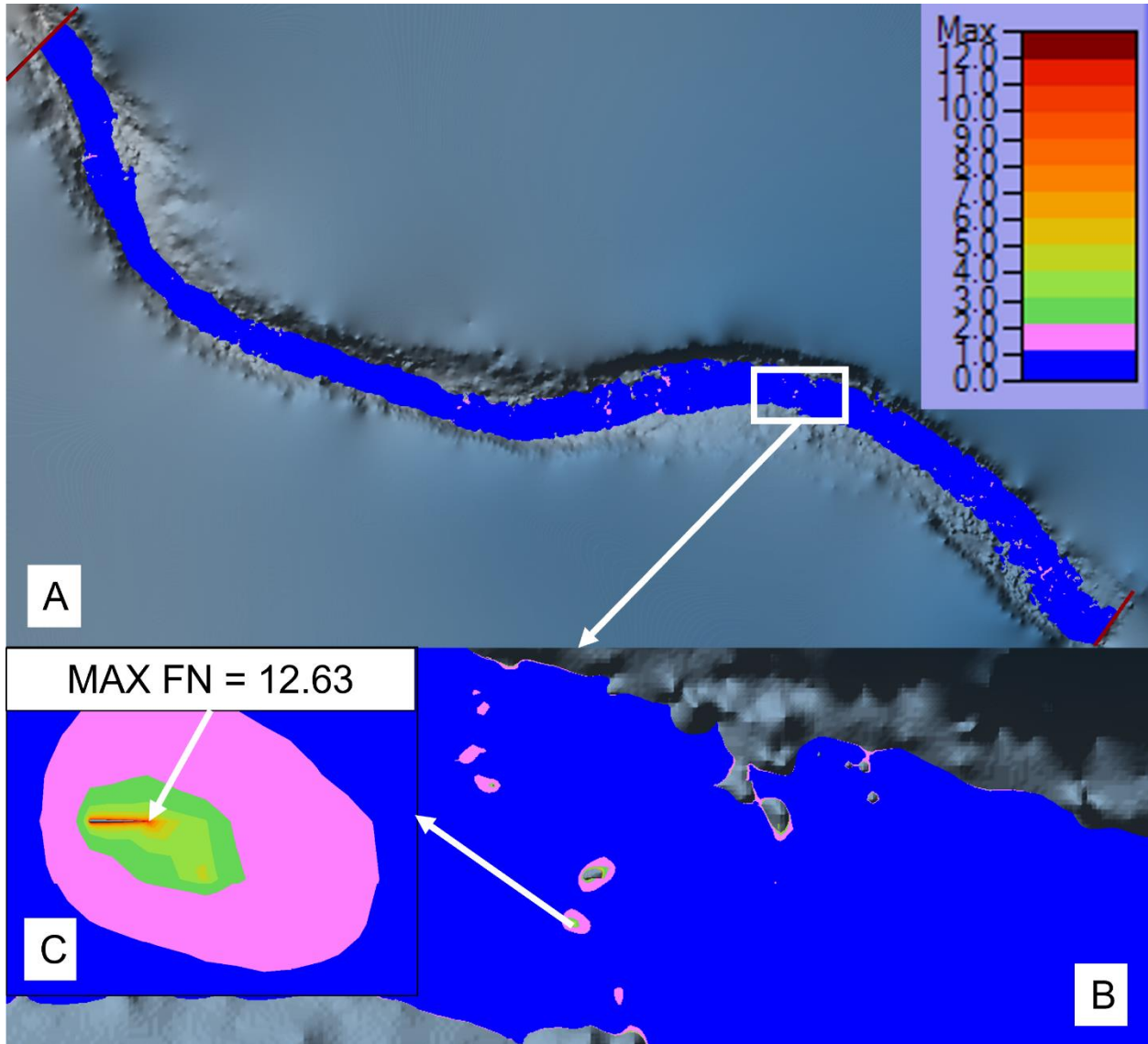


Figure A-18. (A) Site 2 FN display at 70 cfs. (B) Blue cells are FN <1.0, purple, green, and red cells appear sporadically near bed, bank, and substrate boundaries where FN >1.0. (C) Zoomed in on cell with max FN.

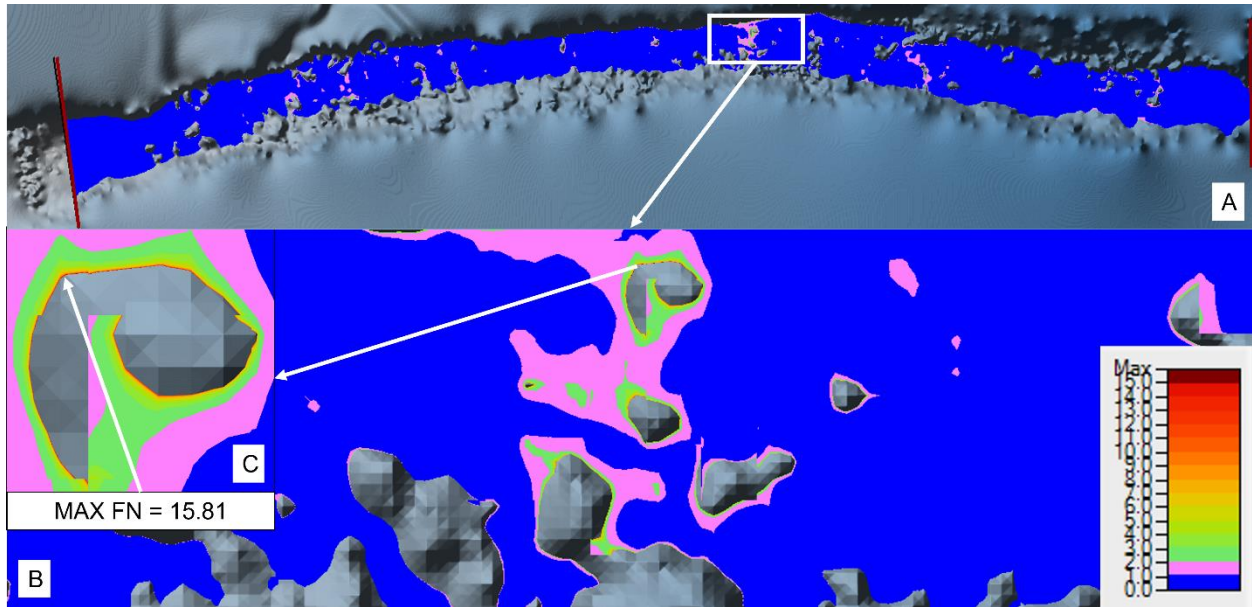


Figure A-19. (A) Site 3 FN display at 17 cfs. (B) Blue cells are FN <1.0, purple, green, and red cells appear sporadically near bed, bank, and substrate boundaries where FN >1.0. (C) Zoomed in on Max cell FN.

A.3.6 HEC-RAS Depth and Velocity Validation Results

Depth and velocity validation data were collected at each site. Validation data were collected at two distinct flows for Sites 1 and 2, and only one flow for Site 3 due to the limited number of storm events in fall 2019 and COVID fieldwork restrictions in 2020 (Table A-21).

Table A-21. Validation discharges.

Site	Date	Flow (cfs)
1	1/10/2019	24.3
1	1/29/2019	4.5
2	1/11/2019	10.5
2	1/30/2019	2.4
2	1/31/2019	2.2
3	4/24/2019	2.0

The validation data locations are plotted on the terrain models output from HEC-RAS for Sites 1, 2, and 3 in Figure A-20, Figure A-21, and Figure A-22, respectively. Validation data for Site 2 at the lower flow were collected over two consecutive days to obtain a representative number of points.

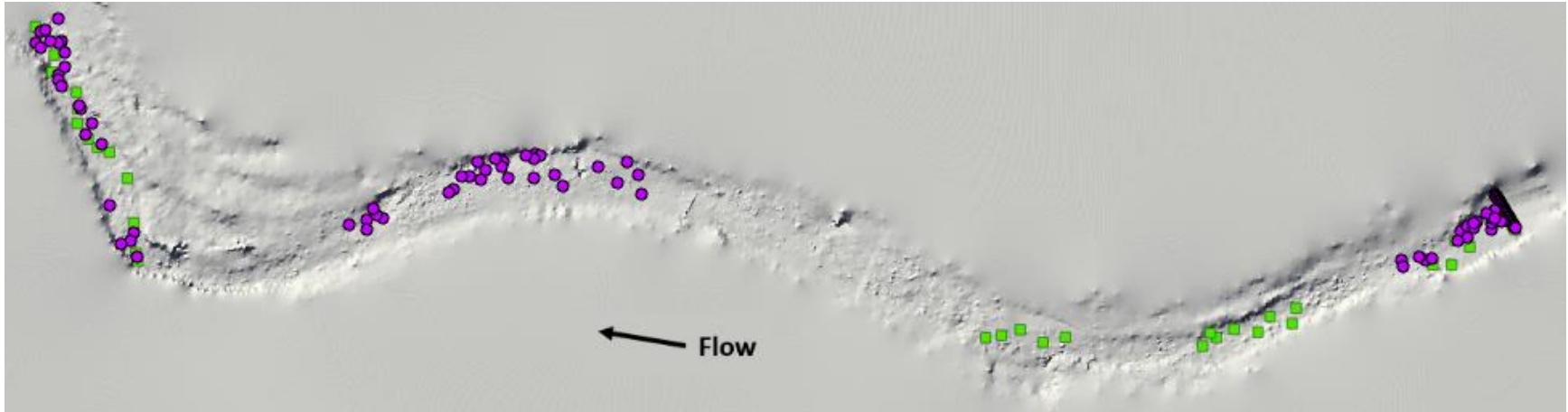


Figure A-20. Site 1 validation data collected at 24.3 cfs (green squares) and at 4.5 cfs (purple circles).

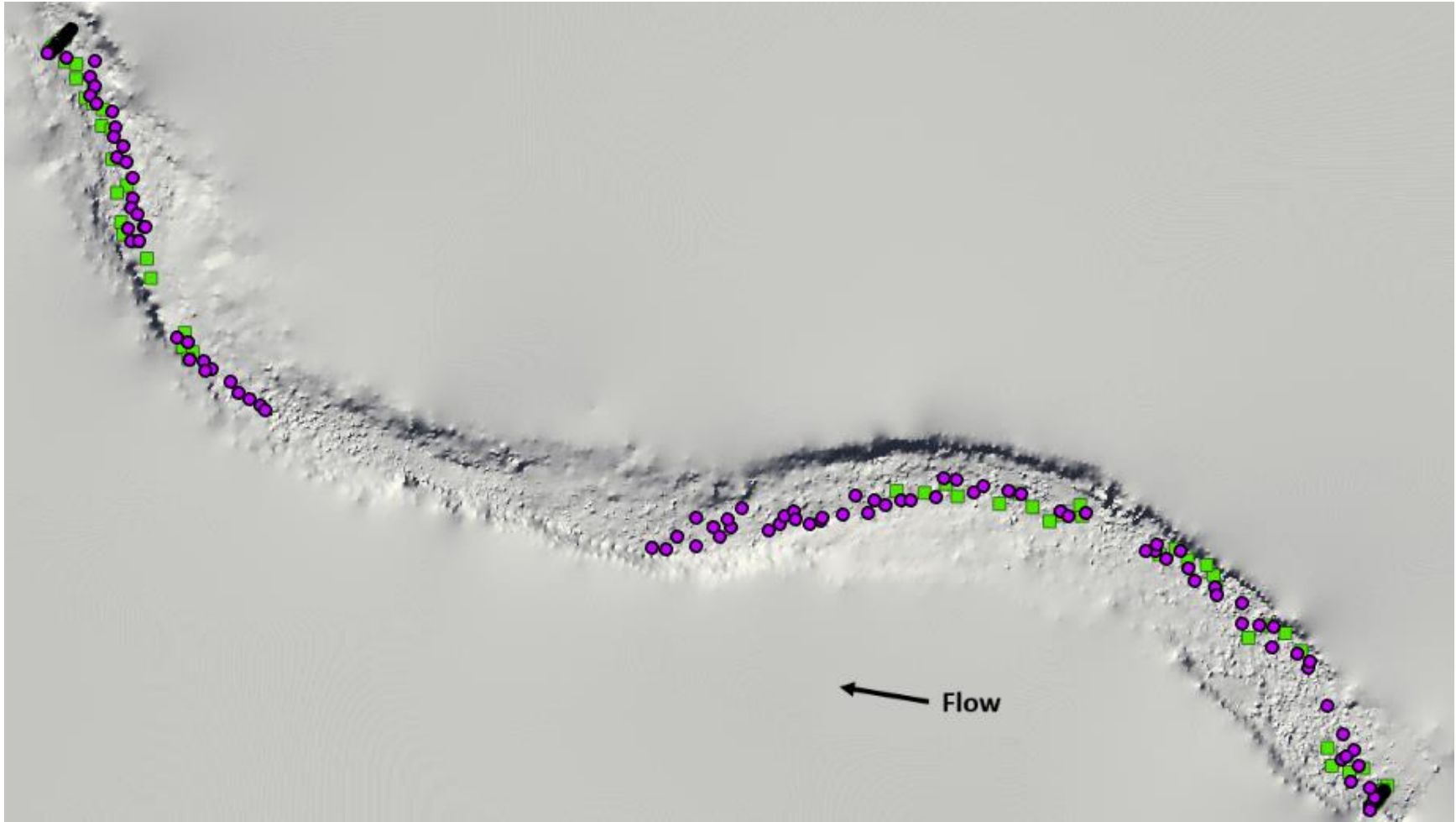


Figure A-21. Site 2 validation data collected at 10.5 cfs (green squares) and at 2.4 and 2.2 cfs (purple circles).

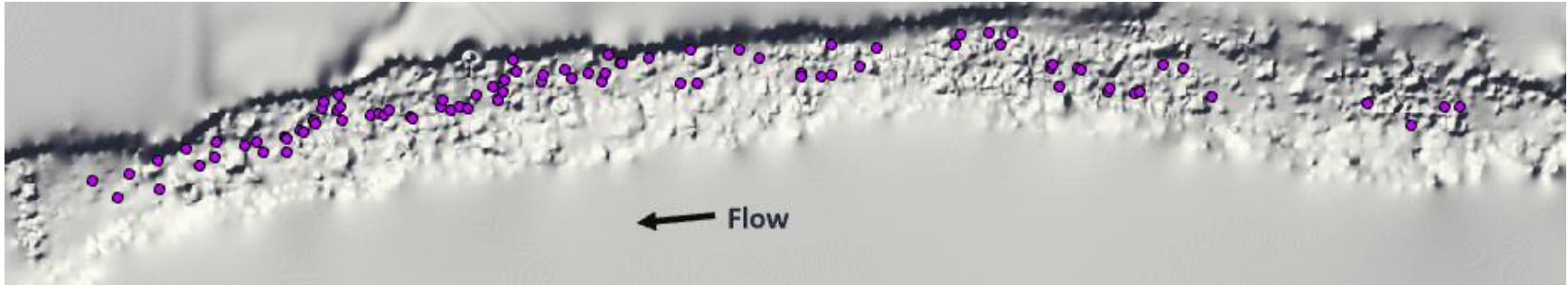


Figure A-22. Site 3 validation data collected at 2.0 cfs (purple circles).

Each flow in Table A-21 was simulated in the HEC-RAS model to generate simulated depths and velocities at each of the validation points. All simulated validation depths and velocities from each site were plotted with the corresponding depths and velocities measured in the field. The simulated and field-measured validation data were further subdivided and replotted by General Mesohabitat Type (Class III). Linear best-fit regression lines were fitted to each plot. The R^2 for each linear best-fit model are reported in Table A-22 through Table A-26 for Sites 1, 2, and 3. The plots containing 'All' validation points are presented below in Figure A-23 through Figure A-32.

Table A-22. Site 1 validation data R^2 values at 24.3 cfs.

Mesohabitat Type	Number of Points	R^2 Depth Values (ft)	R^2 Velocity Values (ft/s)
Riffle	9	0.91	0.51
Pool	16	0.54	0.57
Run	15	0.60	0.26
All	40	0.66	0.56

Table A-23. Site 1 validation data R^2 values at 4.5 cfs.

Mesohabitat Type	Number of Points	R^2 Depth Values (ft)	R^2 Velocity Values (ft/s)
Riffle	30	0.40	0.11
Pool	54	0.76	0.68
Run	10	0.48	0.00
All	94	0.76	0.34

Table A-24. Site 2 validation data R^2 values at 10.5 cfs.

Mesohabitat Type	Number of Points	R^2 Depth Values (ft)	R^2 Velocity Values (ft/s)
Riffle	10	0.43	0.55
Pool	30	0.72	0.29
Run	16	0.63	0.36
All	56	0.72	0.34

Table A-25. Site 2 validation data R² values at 2.2 and 2.4 cfs.

Mesohabitat Type	Number of Points	R ² Depth Values (ft)	R ² Velocity Values (ft/s)
Riffle	35	0.89	0.32
Pool	15	0.51	0.22
Run	48	0.40	0.19
All	98	0.77	0.31

Table A-26. Site 3 validation data R² values at 2.0 cfs.

Mesohabitat Type	Number of Points	R ² Depth Values (ft)	R ² Velocity Values (ft/s)
Pool	42	0.85	0.34
Run	38	0.64	0.05
All	80	0.78	0.14

In general, the validation results fell short of the correlation R² targets for both depth, 0.9, and velocity, 0.6 (USFWS 2011). The riffle and pool units performed better than the run units. Only the depths measured in the riffles of Site 1 at 24.3 cfs correlate above the threshold of 0.9. The riffles in Site 2 at 2.2 and 2.4 cfs were also close to the threshold at 0.89. The average correlation for velocities in Site 1 at 24.3 cfs met the 0.6 threshold helped by the pool unit velocities averaging 0.64. The velocities in the riffles and pools of Site 1 at 4.5 cfs exceeded the 0.6 threshold at 0.79 and 0.73, respectively.

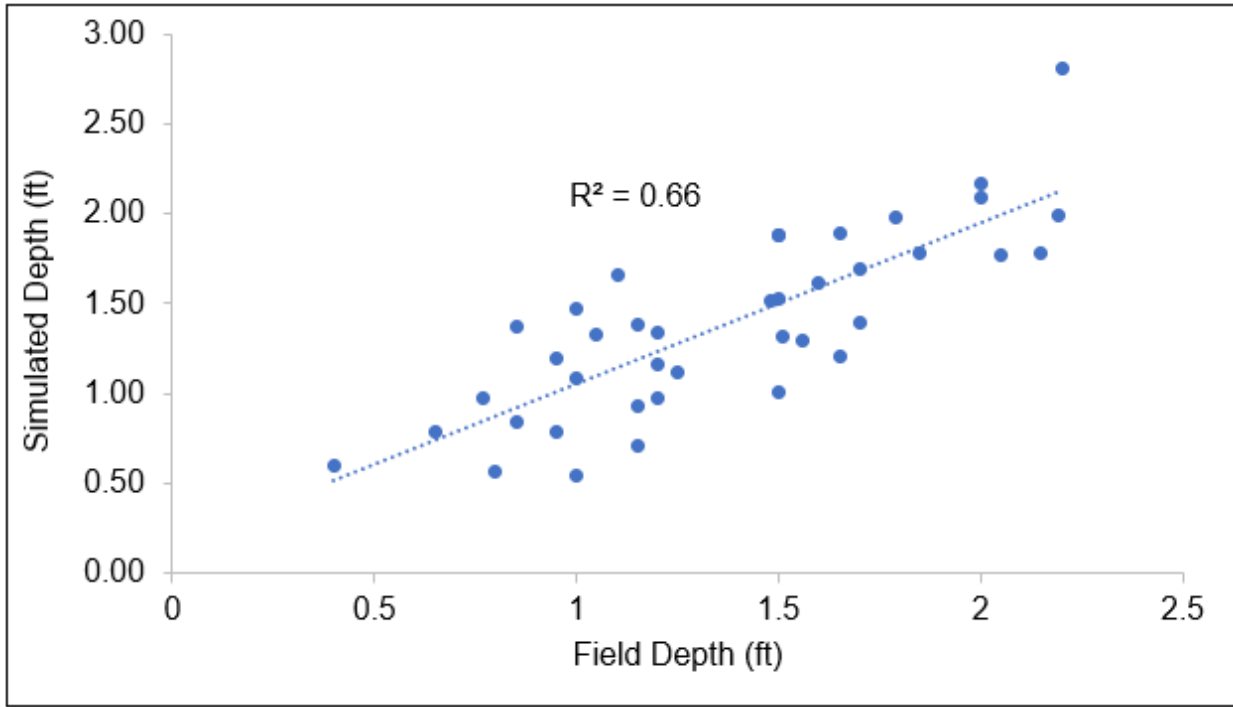


Figure A-23. Site 1, 24.3 cfs depth validation.

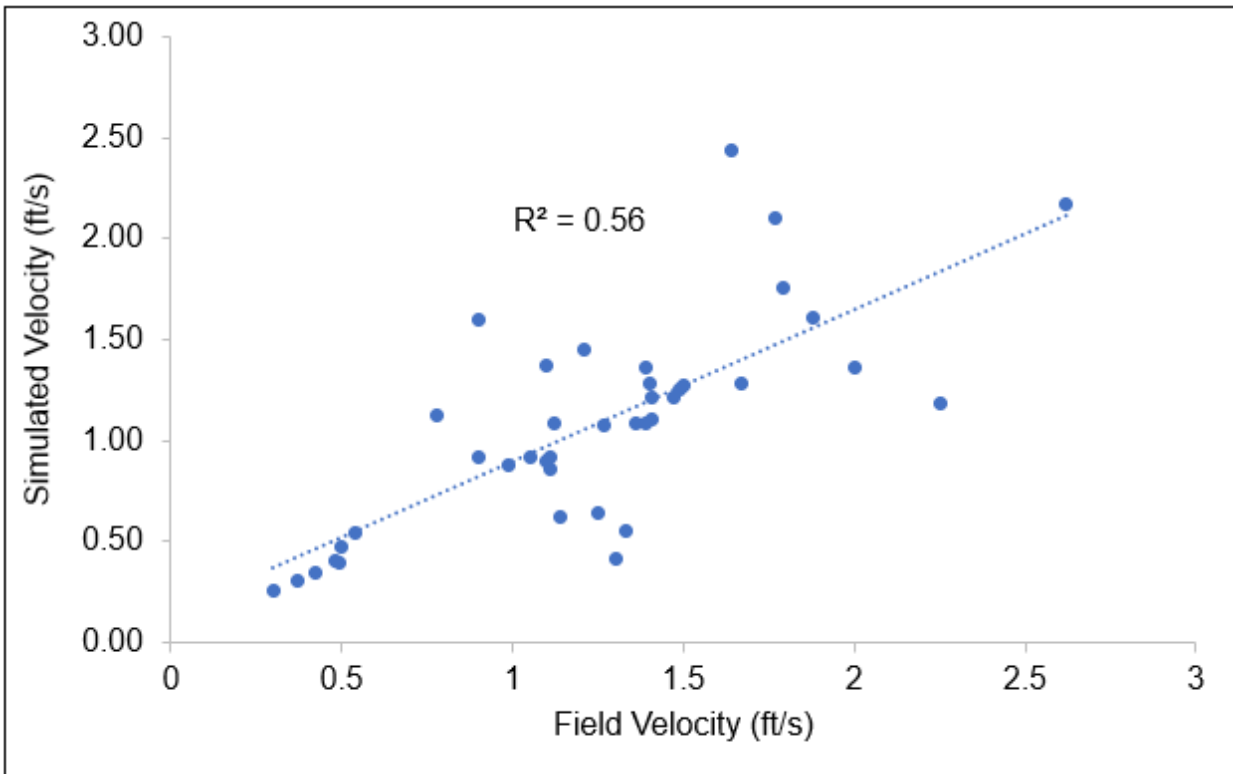


Figure A-24. Site 1, 24.3 cfs velocity validation.

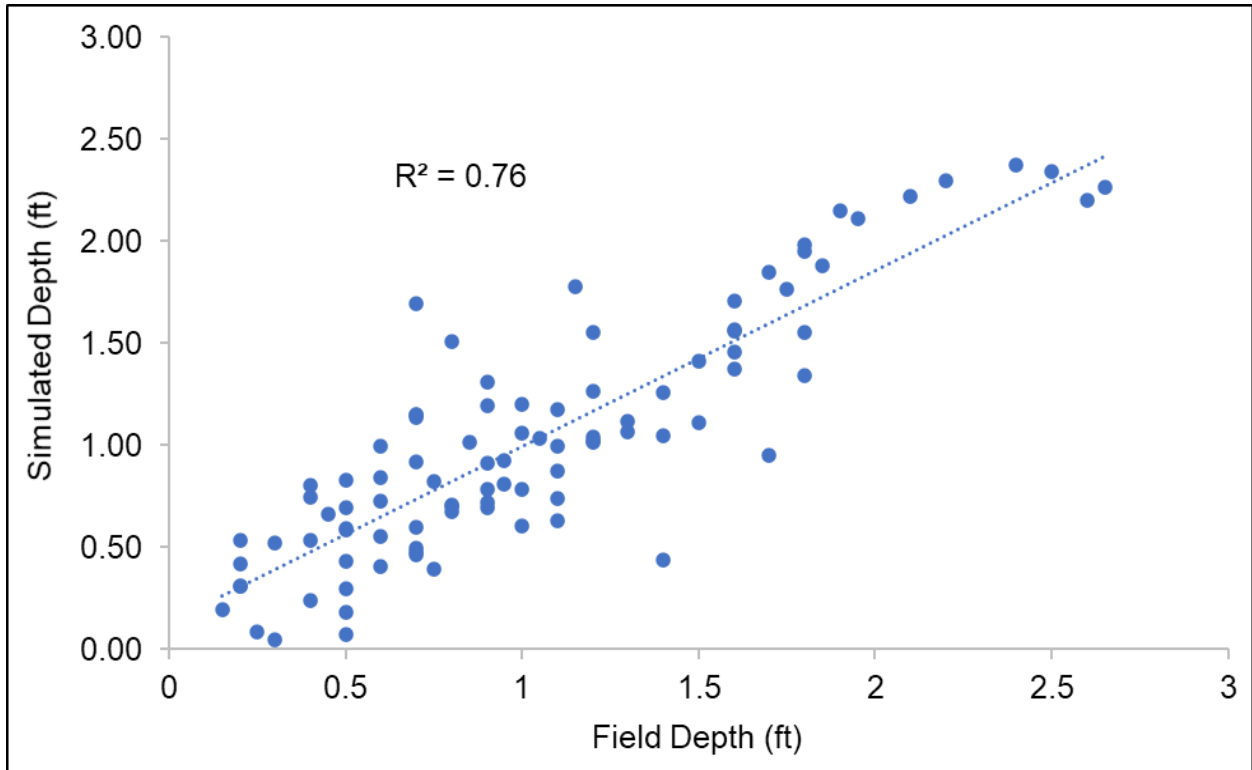


Figure A-25. Site 1, 4.5 cfs depth validation.

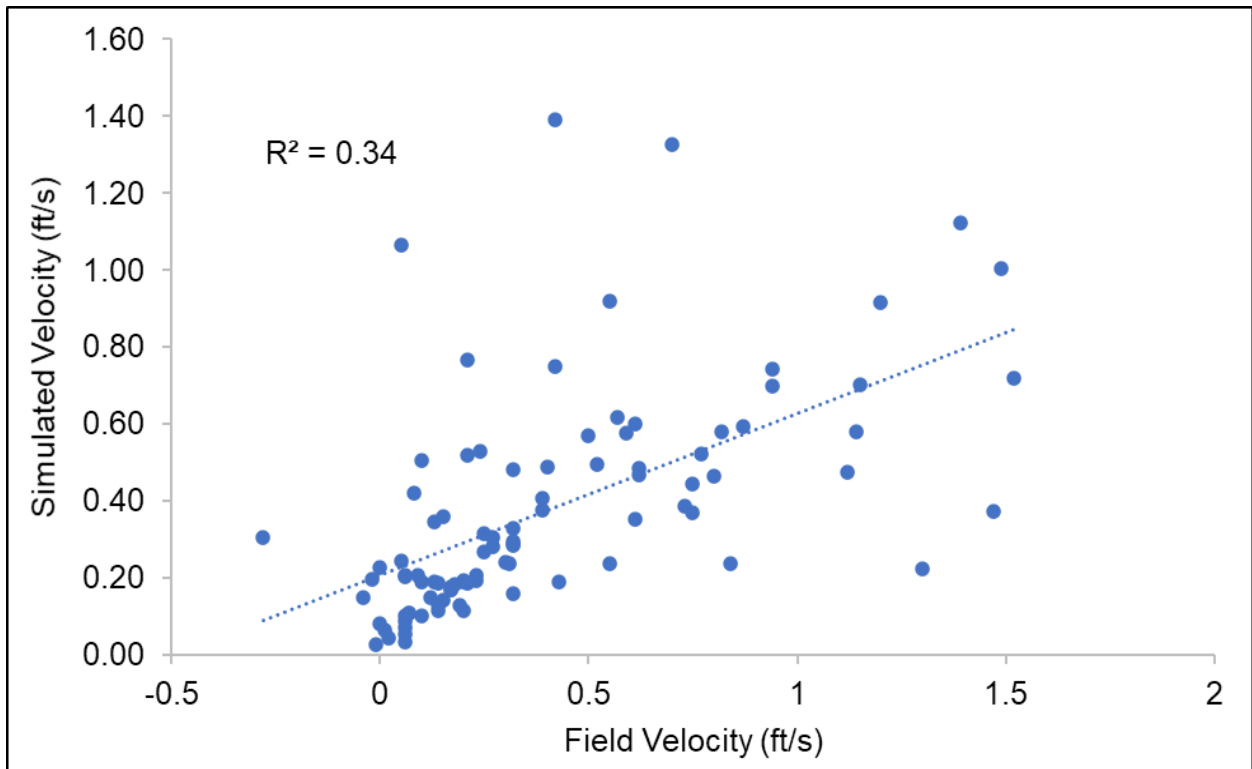


Figure A-26. Site 1, 4.5 cfs velocity validation.

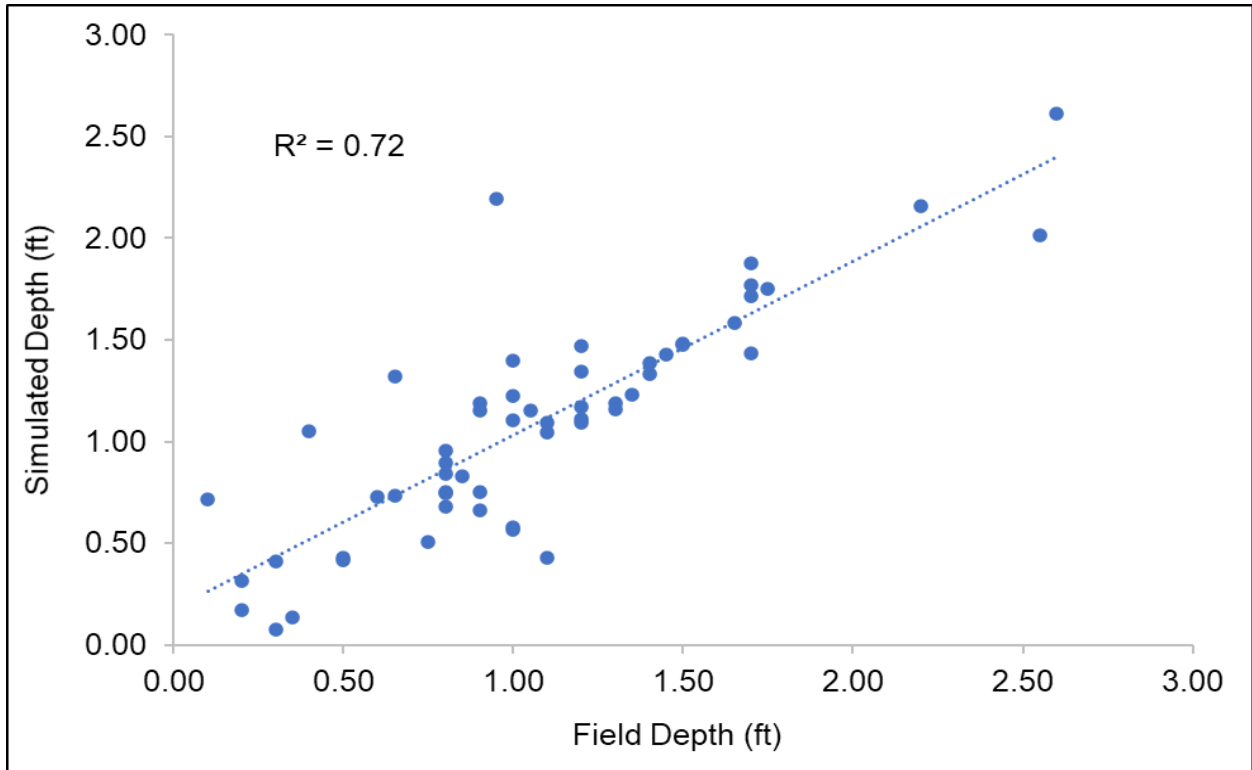


Figure A-27. Site 2, 10.5 cfs depth validation.

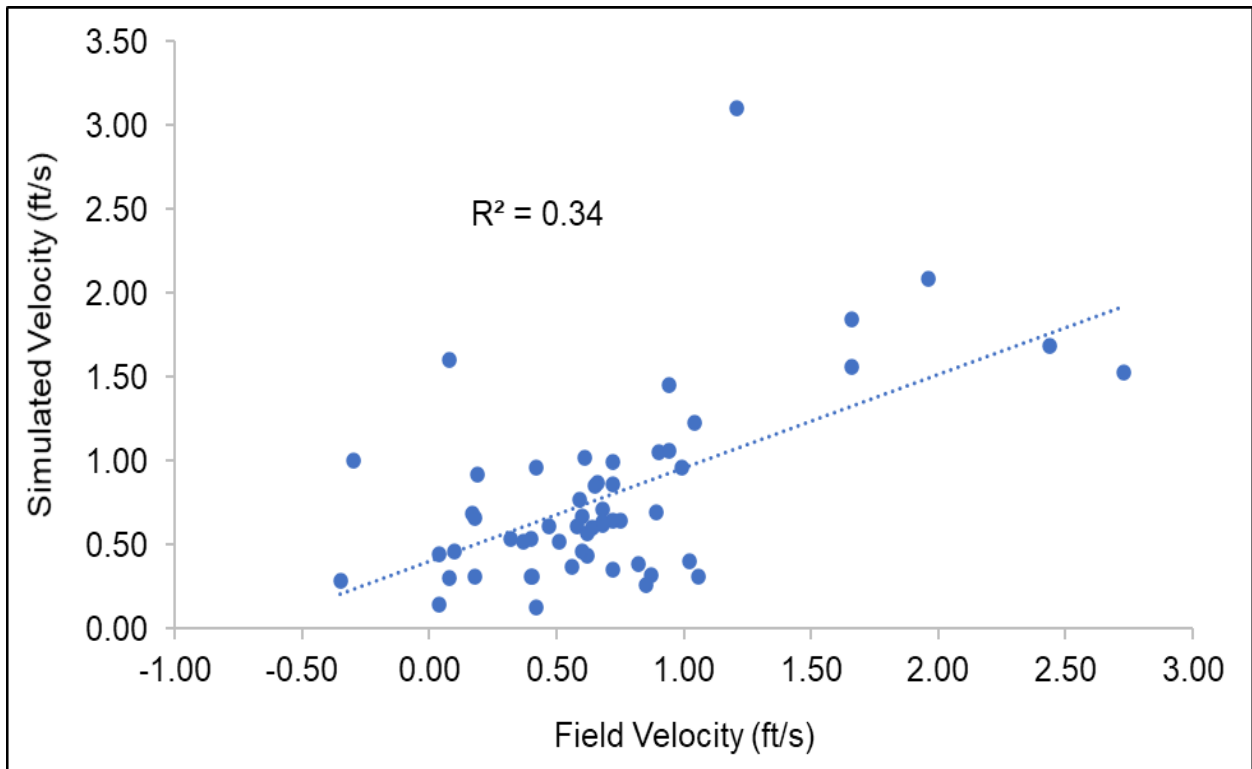


Figure A-28. Site 2, 10.5 cfs velocity validation.

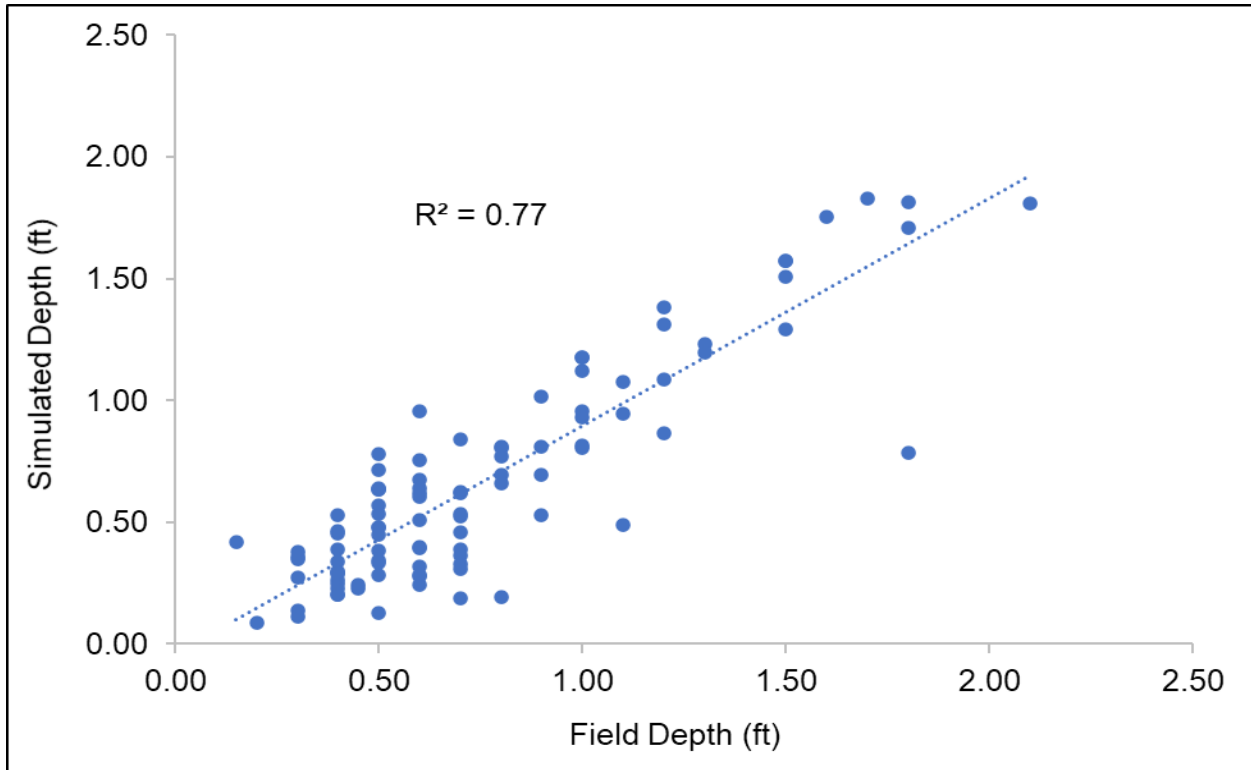


Figure A-29. Site 2, 2.2 and 2.4 cfs depth validation.

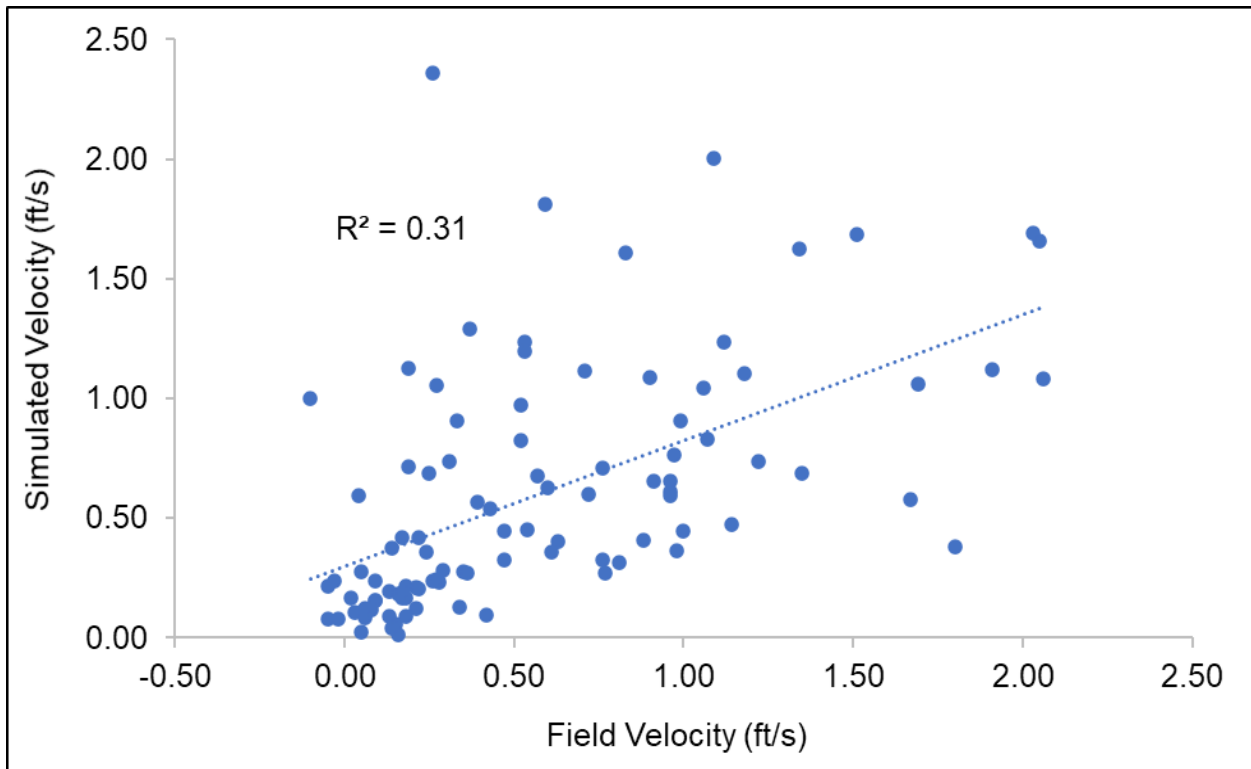


Figure A-30. Site 2, 2.2 and 2.4 cfs velocity validation.

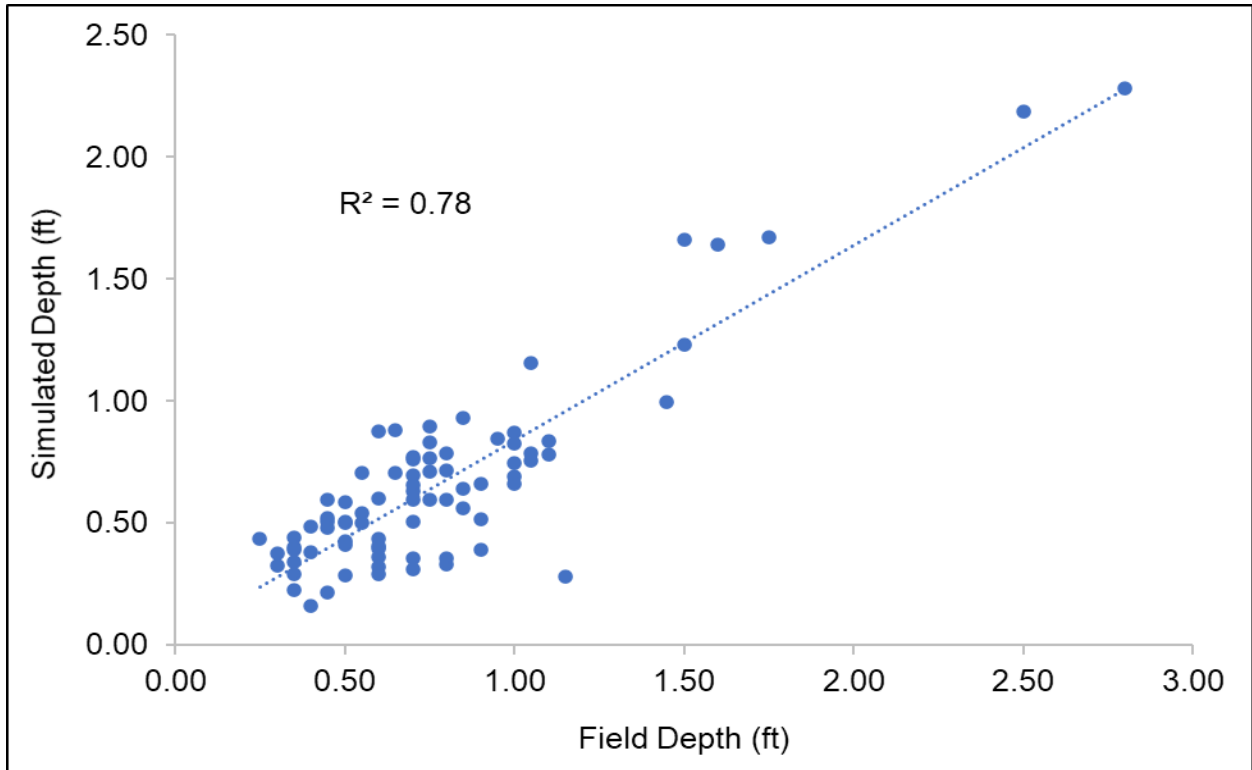


Figure A-31. Site 3, 2.0 cfs depth validation.

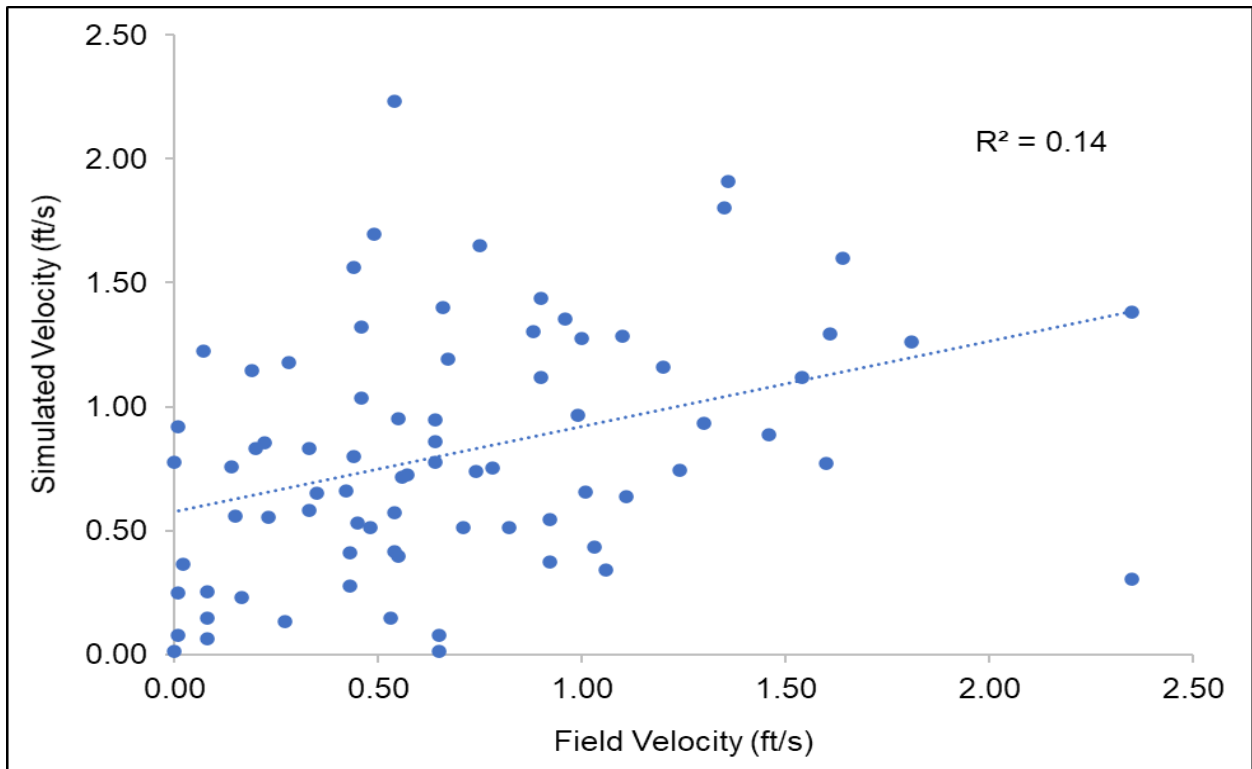


Figure A-32. Site 3, 2.0 cfs velocity validation.

A.4 Discussion

Model calibration was successful for each site. The model outputs for average WSEL at XS-2 of each site were within the recommended threshold of 0.1 ft with the rating curve relationships developed from field-measured data (refer to Table A-13 through Table A-15). Two RMs were required to calibrate flow-WSEL in the Site 1 flow simulations, which ranged from 1 to 70 cfs. Flow-WSEL was calibrated in Sites 2 and 3 using only one RM across the entire simulation flow range. Computational timesteps were reduced when necessary to ensure CN values did not exceed 1.0 for FM solutions and did not exceed 2.0 for DWA solutions (refer to Table A-18 through Table A-20). The net flow threshold, which requires that outflow at equilibrium varies from inflow by less than 1%, were met in all simulations. Model validation consisted of comparing depths and velocities collected at random locations in each study site to simulated values at the same locations. The correlation of the validation field data versus simulated values were varied, especially when categorizing the data by habitat unit type.

A.4.1 Site 1 Roughness Multipliers

Spatial variation in stream bed roughness in each study site was defined by a composite raster of varying n values based on the substrate size code assigned to each topographic survey point. The goal of the flow-WSEL calibration was to apply a single RM to the roughness map for each site to calibrate all the flow simulations. Sites 2 and 3 were calibrated using a single RM over the entire range of simulation flows; Site 2 was calibrated using a single RM of 1.5 and Site 3 was calibrated using a single RM of 1.25. Site 1 required two separate RMs (2.125 and 3.0) to calibrate the model over the range of simulation flows. The RM 2.125 was used to calibrate the model from 10 to 70 cfs. The second RM of 3.0 was only needed to calibrate the model at the lower flow levels of 1 to 5 cfs. A shift in bank profile shape was present between 5 and 10 cfs at XS-2 of Site 1 (Figure A-33). Manning's n is a function of flow cross-sectional area, hydraulic radius and the slope of the water surface, refer to Equation A-2.

As part of the calibration process, the slope of the water surface was computed between XS-2 and the upstream model boundary after each simulation. The slope of the water surface at 5 and 10 cfs was equal, 0.000. The slope of the water surface for the entire length of Site 1 was computed by subtracting the WSEL at XS-2 by the WSEL at XS-1 and dividing that quantity by the stream-length distance between the cross sections (Table A-27).

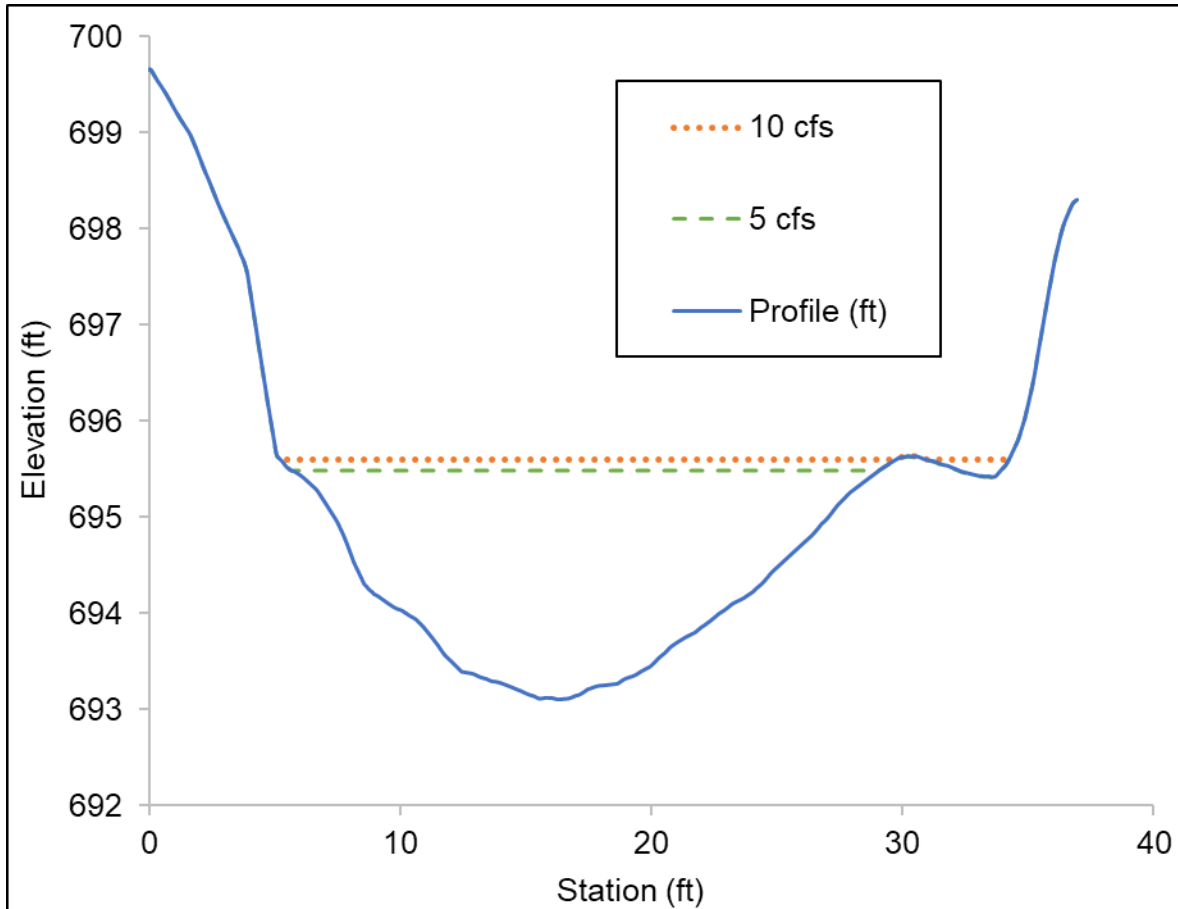


Figure A-33. Site 1, XS-2 elevation profile and average WSELs at 5 and 10 cfs.

Table A-27. Site 1, slope of the water surface.

Flow (cfs)	Slope (ft/ft)
70	0.0115
60	0.0115
50	0.0114
45	0.0114
40	0.0114
35	0.0114
30	0.0114
24.3	0.0113
20	0.0113

Flow (cfs)	Slope (ft/ft)
15	0.0113
10	0.0113
5	0.0114
4.5	0.0114
4	0.0114
3	0.0114
2	0.0114
1	0.0115

The slope of the water surface remained consistent over the flow simulation range, oscillating between 0.0113 and 0.0115. There was a difference of 0.0001 between 5 and 10 cfs, which likely does not indicate the slope of the water surface was a contributor to the change in bed roughness needed to calibrate Site 1 between 10 cfs and 5 cfs. The most likely culprit is the change in shape of the channel at XS-2 in between the WSEL of 5 cfs and 10 cfs (Figure A-33). The change in shape of the channel altered the proportional relationship between the wetted cross-sectional area of the channel and the hydraulic radius (Equation A-2). The efficiency of the channel to convey flow decreased between 5 cfs and 10 cfs, causing the RM to increase from 2.125 to 3.0.

A.4.2 Froude Number

The 2D module of HEC-RAS is a depth-averaging model that uses conservation of mass to solve for velocity in the x- and y-horizontal plane. FN magnitude ($FN < 1$, $FN = 1.0$, and $FN > 1.0$) defines flow transitions from subcritical to critical to supercritical flow, respectively. The transition from subcritical to critical and supercritical flow is characterized by turbulent flow and the onset of vertical mixing. The presence of critical and supercritical flow can disrupt the slope of the water surface elevation used to solve for WSEL using the step-back approach, and result in a poor match between modeled and field-observed WSELs.

Figure A-17 through Figure A-19 highlight the most turbulent areas of the models in terms of FN magnitude. FN values are expected to be less than 1.0 in laminar flow and potentially greater than 1.0 in water flowing over protruding cobbles and boulders (i.e., vertical mixing). FN values greater than 1.0 were only encountered over large-scale submerged rocks and bedrock, around the margins of substrate protruding above the water surface, and sporadically along wetted stream margins. Supercritical flow would be expected in these types of situations. The model simulated FN values above 1.0 in Sites 1 and 2 around substrate protruding above the water surface, and sporadically along wetted stream margins (Figure A-17 and Figure A-18, respectively).

In Site 3, HEC-RAS simulated isolated areas of high FN values, ranging from 1.0 to 2.0, over large-scale submerged substrate (Figure A-19). Figure A-34 through Figure A-36 provide examples of the substrate sizes observed in each site. The average substrate size increased from Site 1 to Site 3 (Table A-1). The magnitude of FN values in the most turbulent portions of the models is consistent with the range of substrate sizes observed by staff in each site.

However, the presence of FN values above 1.0 in Site 3 does not appear to have impacted the flow-WSEL calibration. The flow-WSEL rating R^2 values for both XS-1 and XS-2 in Site 3 were greater than 0.999, surpassing standard expectations.

A.4.3 Depth and Velocity Validation Results

The depth and velocity validation results from all three sites were varied. Review of each site shows that all three sites possessed cobbles, boulders, and bedrock outcroppings. This larger substrate causes complex hydraulics including vertical mixing of flow (refer to Figure A-34, Figure A-35, and Figure A-36 for Sites 1, 2, and 3, respectively).



Figure A-34. Example of Site 1 sand, gravel, cobbles, and boulders.



Figure A-35. Example of Site 2 gravel, cobbles, and boulders.



Figure A-36. Example of Site 3 gravel, cobbles, boulders, and bedrock.

2D models conserve mass and momentum by solving for depth in the vertical z-direction and velocity only in the x- and y-direction. 2D models assume velocities in the z-direction are small compared with the horizontal direction. If mass and momentum in the vertical direction exist in the field stream dynamics, by default the magnitude of that mass and momentum must be expressed by adding or subtracting the magnitude of depth in the z-direction or velocity of the x- and y-directions. The presence of vertical mixing in the study sites could have affected the accuracy of the model estimates of depth and velocity.

REFERENCES

- Bray, D. I. (1979). Estimating average velocity in gravel-bed rivers. *American Society of Civil Engineers* **105**(No. HY9): 1103-1122.
- Chow, V. T. (1959). *Open-channel hydraulics*. In. McGraw-Hill, NY. pp. 680.
- Coon, W. F. (1998). Estimation of roughness coefficients for natural stream channels with vegetated banks. U.S. Geological Survey, Department of the Interior; prepared in cooperation with the New York State Department of Transportation, Denver, CO. Water-supply paper 2441.
- ESRI (2020). ArcGIS Pro 2.8: Create Thiessen polygons (analysis) [Internet], ESRI.
- Friend, A., P.E. and M. McBroom, P.E. (2018). Smooth transition: Adjusting Manning's n values for 2D modeling [presentation]. Michael Baker International, Great Falls, MT.
- Gupta, R. S. (1995). *Hydrology and hydraulic systems*. Waveland Press, Inc., Prospect Heights, IL.
- HEC-RAS (2018). Version 5.0.6 [computer software]. Davis, CA, U.S. Army Corps of Engineers, Hydraulic Engineering Center.
- Jobson, H. E. and D. C. Froehlich (1988). *Basic hydraulic principles of open-channel flow*. U.S. Geological Survey, Department of the Interior (USGS), Reston, VA. Open-File Report 88-707.
- Milhous, R. T., M. A. Updike and D. M. Schneider (1989). *Physical Habitat Simulation System reference manual - version II*. U.S. Fish and Wildlife Service, Fort Collins, CO. Instream flow information paper 26, Biological report 89(16).
- Munson, B. R., D. F. Young and T. H. Okiishi (1998). *Fundamentals of fluid mechanics*. 3rd edition. John Wiley & Sons Inc.
- USACE (2016). HEC-RAS river analysis system. Hydraulic reference manual. Version 5.0. U.S. Army Corps of Engineers, Hydrologic Engineering Center (USACE), Davis, CA. Available: <https://www.hec.usace.army.mil/software/hecras/documentation/HEC-RAS%205.0%20Reference%20Manual.pdf>.
- USFWS (2011). *Sacramento Fish and Wildlife Office standards for Physical Habitat Simulation studies*. U.S. Fish and Wildlife Service, Sacramento Fish and Wildlife Office, Restoration and Monitoring Program (USFWS), Sacramento, CA.
- Waddle, T. (2001). *PHABSIM for Windows, user's manual and exercises*. U.S. Geological Survey, Midcontinent Ecological Science Center (USGS), Fort Collins, CO. Open File Report 01-340.

WEST Consultants Inc (2017). Two-dimensional modeling using HEC-RAS. HEC-RAS 5.0 Workshop.

APPENDIX B: FIELD OBSERVATIONS

Examples of study transects in Site 1, Site 2, and Site 3 are provided in the paired figures below (Figure B-1 to Figure B-14). Each figure contrasts conditions at the Low and High flows used as inputs to the 2D models, as well as trail camera photos comparing Low, Medium, and High flows.

B.1 Site 1

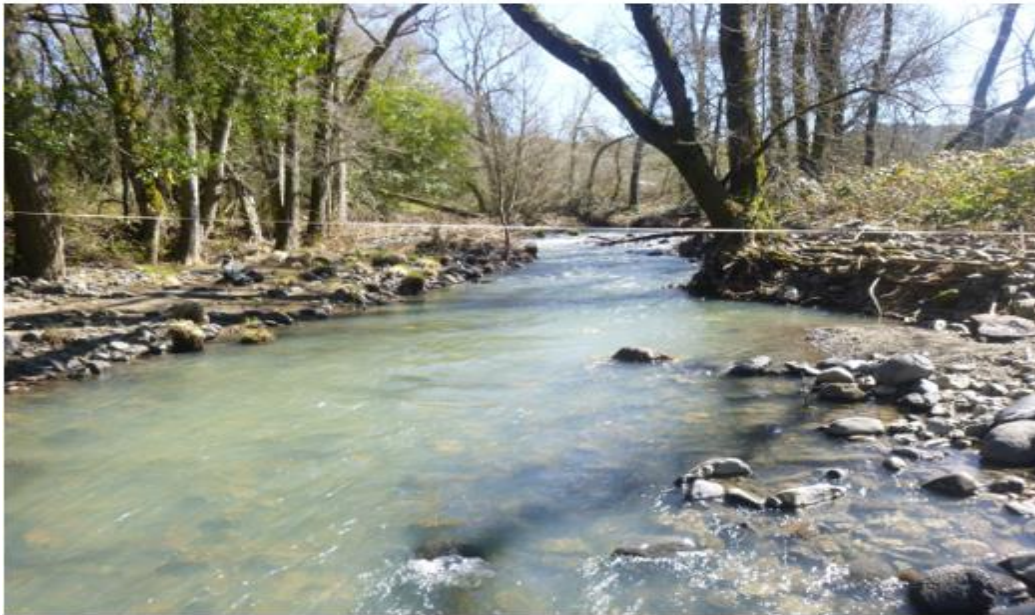


Figure B-1. Upstream view of XS-1 (Site 1) at 3.2 cfs (upper photo, 4/24/2018) and 21.8 cfs (lower photo, 3/12/2019).



Figure B-2. Downstream view of XS-2 (Site 1) at 3.2 cfs (upper photo, 4/24/2018) and 13.8 cfs (lower photo, 1/11/2019).



Figure B-3. Upstream view of XS-2 (Site 1) at 1.2 cfs (upper photo, 5/16/2018) and 21.8 cfs (lower photo, 3/13/2019).



Figure B-4. Site 1 trail camera photos at Low, Mid, and High flow. The photo at Low flow has a slightly different field of view.

B.2 Site 2

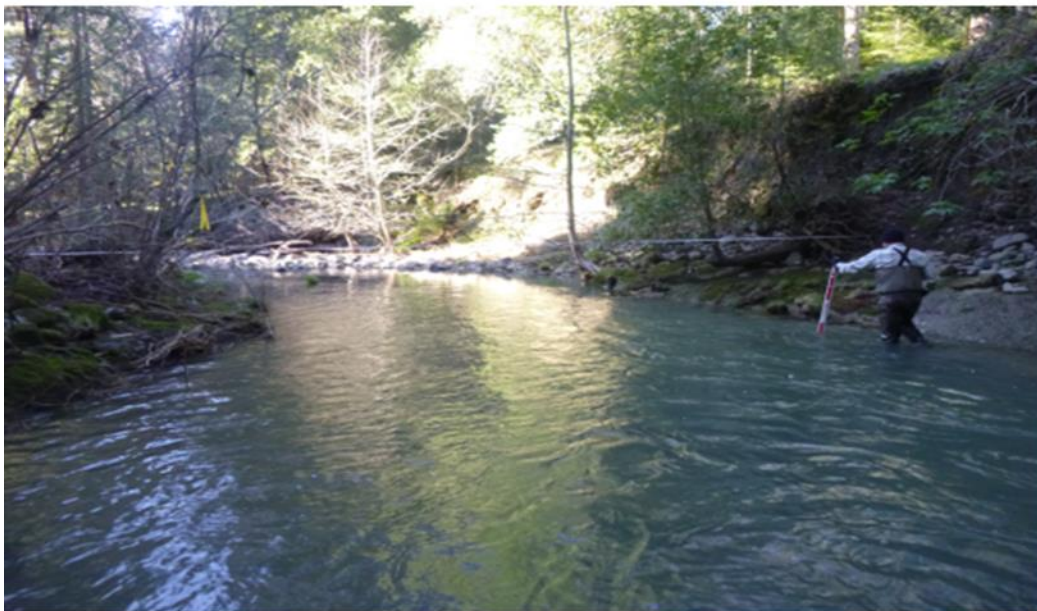


Figure B-5. Downstream view of XS-1 (Site 2) at 5.3 cfs (upper photo, 4/16/2018) and 12.9 cfs (lower photo, 3/13/2019).



Figure B-6. Upstream view of XS-1 (Site 2) at 1.6 cfs (upper photo, 4/25/2018) and 26.3 cfs (lower photo, 1/18/2019).



Figure B-7. Upstream view of XS-2 (Site 2) at 0.8 cfs (upper photo, 5/16/2018) and 12.9 cfs (lower photo, 3/13/2019).



Figure B-8. Downstream view of discharge location (Site 2) at 1 cfs (upper photo, 12/05/2018) and 12.9 cfs (lower photo, 3/13/2019).



Figure B-9. Upstream view towards discharge location (Site 2) at 2.5 cfs (upper photo, 12/10/2019) and 26.3 cfs (lower photo, 1/18/2019).



Figure B-10. Site 2 trail camera photos at Low, Mid, and High flow.

B.3 Site 3



Figure B-11. Downstream view of XS-1 (Site 3) at 2.9 cfs (upper photo, 4/17/2018) and 8.1 cfs (lower photo, 3/14/2019).



Figure B-12. Downstream view of XS-2 (Site 3) at 0.5 cfs (upper photo, 5/16/2018) and 6.8 cfs (lower photo, 1/11/2019).



Figure B-13. Upstream view of XS-2 (Site 3) at 2.9 cfs (upper photo, 4/17/2018) and 8.1 cfs (lower photo, 3/14/2019).



Figure B-14. Site 3 trail camera photos at Low, Mid, and High flow.

APPENDIX C: STREAMFLOW–HABITAT TABLES

The following appendix shows the estimated AWS values for each species and life stage by study site.

Table C-1. Site 1 upper Mark West Creek steelhead and Coho Salmon streamflow/habitat relationships. Peak AWS percentage values for each life stage are bolded in grey with a dagger.

Discharge (cfs)	AWS for Coho Salmon Fry (<6 cm)	AWS for Coho Salmon Juveniles (≥6 cm)	AWS for Steelhead Fry (<6 cm)	AWS for Steelhead Juveniles (≥6 cm)
1	96.4	90.2	90.3	30.2
2	100.0†	97.2	97.8	37.4
3	99.8	99.7	100.0†	43.1
4	98.2	100.0†	99.9	47.9
5	95.7	99.2	98.8	52.5
10	67.9	74.5	74.3	65.2
15	54.1	61.4	61.6	77.2
20	44.4	51.5	52.0	85.7
30	31.8	38.4	39.0	95.8
35	27.8	34.1	34.6	98.3
40	24.7	30.7	31.1	99.6
45	22.5	28.0	28.4	100.0†
50	20.8	25.9	26.2	99.8
60	19.2	23.3	23.7	98.2
70	18.9	21.8	22.7	95.8

Table C-2. Site 2 upper Mark West Creek steelhead and Coho Salmon streamflow/habitat relationships. Peak AWS percentage values for each life stage are bolded in grey with a dagger.

Discharge (cfs)	AWS for Coho Salmon Fry (<6 cm)	AWS for Coho Salmon Juveniles (≥6 cm)	AWS for Steelhead Fry (<6 cm)	AWS for Steelhead Juveniles (≥6 cm)
1	100.0†	97.7	97.8	31.1
2	98.2	100.0†	100.0†	39.9
3	94.4	99.0	98.1	47.0
4	90.5	96.8	95.0	52.9
5	86.6	94.1	91.6	58.4
10	69.6	79.3	75.9	77.1
15	59.2	68.1	65.6	88.1
20	51.9	59.7	58.2	94.3
25	46.3	53.1	52.5	97.9
30	41.9	48.1	48.1	99.6
35	38.4	44.4	44.6	100.0†
40	35.3	41.2	41.4	99.4
50	31.3	36.6	36.7	96.5
60	28.7	33.5	33.6	92.4
70	27.0	31.2	31.4	87.9

Table C-3. Site 3 upper Mark West Creek steelhead and Coho Salmon streamflow/habitat relationships. Peak AWS percentage values for each life stage are bolded in grey with a dagger.

Discharge (cfs)	AWS for Coho Salmon Fry (<6 cm)	AWS for Coho Salmon Juveniles (≥6 cm)	AWS for Steelhead Fry (<6 cm)	AWS for Steelhead Juveniles (≥6 cm)
1	100.0†	98.6	100.00†	38.0
2	95.1	100.0†	98.9	50.3
3	89.5	97.8	94.5	59.5
4	84.5	94.7	89.5	66.7
5	80.0	91.5	85.0	72.8
10	65.3	78.6	69.5	90.4
15	54.1	67.7	58.6	97.9
17	50.8	64.1	55.1	99.2
18	49.2	62.4	53.5	99.6
19	47.8	60.9	52.0	99.9
20	46.4	59.6	50.7	100.0†
21	45.1	58.2	49.3	100.0
22	43.9	56.9	48.0	99.9
25	40.9	53.4	44.4	99.1
30	37.0	49.2	40.0	96.3
40	32.0	43.4	33.9	88.4
50	28.9	39.4	30.3	80.1